

## Chapter 12

### **The Channel-Hillslope Integrated Landscape Development Model (CHILD)**

Gregory E. Tucker<sup>1</sup>, Stephen T. Lancaster<sup>2</sup>, Nicole M. Gasparini, and Rafael L. Bras

*Department of Civil and Environmental Engineering, Massachusetts Institute of Technology, Cambridge, MA USA*

#### **1. INTRODUCTION**

Numerical models of complex Earth systems serve two important purposes. First, they embody quantitative hypotheses about those systems and thus help researchers develop insight and generate testable predictions. Second, in a more pragmatic context, numerical models are often called upon as quantitative decision-support tools. In geomorphology, mathematical and numerical models provide a crucial link between small-scale, measurable processes and their long-term geomorphic implications. In recent years, several models have been developed that simulate the structure and evolution of three-dimensional fluvial terrain as a consequence of different process “laws” (e.g., Willgoose et al., 1991a; Beaumont et al., 1992; Chase, 1992; Anderson, 1994; Howard, 1994; Tucker and Slingerland, 1994; Moglen and Bras, 1995). By providing the much-needed connection between measurable processes and the dynamics of long-term landscape evolution that these processes drive, mathematical landscape models have posed challenging new hypotheses and have provided the guiding impetus

<sup>1</sup> Now at: School of Geography and the Environment, University of Oxford, Mansfield Road, Oxford OX1 3TB United Kingdom, email: [greg.tucker@geog.ox.ac.uk](mailto:greg.tucker@geog.ox.ac.uk)

<sup>2</sup> Now at: Department of Geosciences, Oregon State University, Corvallis, OR

behind new quantitative field studies and DEM-based analyses of terrain (e.g., Snyder et al., 2000). The current generation of models, however, shares a number of important limitations. Most models rely on a highly simplified representation of drainage basin hydrology, treating climate through a simple “perpetual runoff” formulation. The role of sediment sorting and size-dependent transport dynamics has been ignored in most studies of drainage basin development, despite its importance for understanding the interaction between terrain erosion and sedimentary basin deposition (e.g., Gasparini et al., 1999; Robinson and Slingerland, 1998). Furthermore, with the exception of the pioneering work of Braun and Sambridge (1997), the present generation of models is inherently two-dimensional, describing the dynamics of surface evolution solely in terms of vertical movements without regard to lateral displacement by tectonic or erosional processes.

Our aim in this paper is to present an overview of the Channel-Hillslope Integrated Landscape Development (CHILD) model, a new geomorphic modeling system that overcomes many of the limitations of the previous generation of models and provides a general and extensible computational framework for exploring research questions related to landscape evolution. We focus here on reviewing the underlying theory and illustrating the capabilities of the model through a series of examples. Discussion of the technical details of implementation is given by Tucker et al. (1999, 2000) and Lancaster (1998). We begin by briefly reviewing previous work in landscape evolution modeling. We then discuss the theory and capabilities of the modeling system, and present a series of examples that highlight those capabilities and yield some useful insights into landscape dynamics.

## 2. BACKGROUND

The first quantitative geomorphic process models began to appear in the 1960s, stimulated by the combination of an intellectual shift toward investigating the mechanics of erosion and sedimentation processes, and the appearance of digital computers. The earliest models were one-dimensional slope simulations developed to explore basic concepts in hillslope profile development (e.g., Culling, 1960; Scheidegger, 1961; Ahnert, 1970; Kirkby, 1971; Luke, 1972; Gossman, 1976). These studies helped to quantify and formalize some of the concepts of hillslope process and form enunciated by early workers such as Gilbert (1877) and Penck (1921). Similar one-dimensional (1D) approaches have more recently been used to examine the evolution of stream profiles (e.g., Snow and Slingerland, 1987) and alluvial deposystems (e.g., Paola et al., 1992; Robinson and Slingerland, 1998). There are clear limitations of the 1D approach for understanding terrain

morphology, however, and these limitations prompted early efforts to extend erosion models to two dimensions, though still with a focus primarily on hillslope morphology (Ahnert, 1976; Armstrong, 1976; Kirkby, 1986).

Driven in part by technological advances, there has been a flowering of landscape evolution models during the past decade. Many of these models have focused on watershed evolution and dynamics (Willgoose et al., 1991a; Howard, 1994; Moglen and Bras, 1995; Coulthard et al., 1997; Tucker and Slingerland, 1997; Densmore et al., 1998). Although spatial scale is often not specified, these modeling studies have generally focused on the formation of hillslope-valley topography within small- to moderate-sized drainage basins (on the order of several square kilometers or smaller). In parallel with these developments in watershed geomorphology, a number of researchers have attempted to model the evolution of terrain on the scale of a mountain range or larger (e.g., Koons, 1989; Beaumont et al., 1992; Lifton and Chase, 1992; Anderson, 1994; Tucker and Slingerland, 1994, 1996; Braun and Sambridge, 1997). In these applications, computational limitations dictate the use of a coarse spatial discretization in which individual grid cells are much larger than the scale of an individual hillslope, making it impossible to address explicitly the role of hillslope dynamics, and raising the issue of “upscaling” as a need in large-scale geomorphic models (Howard et al., 1994). A third category of models includes cellular statistical-physical models that employ simple rule sets to address the origin and nature of scaling properties observed in river networks and terrain (e.g., Chase, 1992; Rigon et al., 1994; Rodriguez-Iturbe and Rinaldo, 1997). Finally, a number of two-dimensional models of hillslope-scale soil erosion and rill development have been developed to study and predict patterns of slope erosion and drainage pattern initiation (e.g., Smith and Merchant, 1995; Favis-Mortlock, 1998; Mitas and Mitasova, 1998).

Despite significant progress in theory and model development over the past decade, the current generation of physically based models suffers from several limitations: (1) temporal variability in rainfall and runoff has been largely ignored (cf. Tucker and Bras, 2000); (2) with a few exceptions (e.g., Ijjasz-Vasquez et al., 1992; Tucker and Bras, 1998), runoff is usually treated as spatially uniform (Hortonian) across the landscape, despite the well known importance of variable source-area runoff generation in humid regions; (3) lateral erosion by channels has been ignored in the context of drainage basin evolution; (4) most models use a fixed and uniform spatial discretization in which only vertical movements of the terrain surface are allowed (for an exception, see Braun and Sambridge, 1997); (5) the role of heterogeneous sediment and sorting dynamics is usually ignored for simplicity, despite their potential impacts on stream profile shape (e.g.,

Snow and Slingerland, 1987; Sinha and Parker, 1996; Robinson and Slingerland, 1998) and drainage basin structure (Gasparini et al., 1999); and (6) few efforts have been made to examine the coupling between erosional and depositional systems (e.g., Johnson and Beaumont, 1995; Tucker and Slingerland, 1996; Densmore et al., 1998).

### 3. MODEL FORMULATION

#### 3.1 Overview

The CHILD model simulates the evolution of a topographic surface and its subjacent stratigraphy under a set of driving erosion and sedimentation processes and with a prescribed set of initial and boundary conditions (Fig. 1). Designed to serve as a computational framework for investigating a wide range of problems in catchment geomorphology, CHILD is both a model, in the sense that it comprises a set of hypotheses about how nature works, and a software tool, in the sense that it provides a simulation environment for exploring the consequences of different hypotheses, parameters, and boundary conditions. Here we will use the term “model” to refer collectively to the software and the assumptions and hypotheses embedded within it.

The process modules in CHILD are summarized graphically in Figure 2. Processes incorporated in the model include: (1) climate forcing via a sequence of discrete storm events with durations, intensities, and inter-arrival times that may be either random or constant; (2) generation of runoff by infiltration-excess or saturation-excess mechanisms; (3) downslope routing of water and sediment using a steepest-descent method; (4) detachment (erosion) of sediment or bedrock by channelized surface runoff in rills or stream channels; (5) water-borne downslope transport of detached sediment; (6) transport of sediment by soil creep and related processes on hillslopes; (7) meandering of large stream channels; (8) overbank sedimentation on floodplains; and (9) tectonic deformation. Note that not all of these processes need to be, or even should be, considered in any particular application. The point of including a number of different processes is to allow one to investigate different types of geomorphic system under different space and time scales, using a common modeling framework that handles the basic spatial and temporal simulation framework.

In addition to these process modules, CHILD includes capabilities for managing the spatial simulation framework. The use of an adaptive, irregular spatial discretization adds several useful capabilities (Braun and Sambridge, 1997; Tucker et al., 2000), including the ability to vary spatial resolution and

to incorporate the horizontal components of erosion processes (e.g., stream channel migration) and tectonic motions (e.g., strike-slip displacement). In addition, the model can simulate depositional history and stratigraphy by tracking and updating “layers” of deposited material underlying each point in the landscape, thereby making it possible to model coupled erosion-deposition systems such as mountain drainage basins and their associated alluvial fans (e.g., Ellis et al., 1999).

### 3.2 Continuity of Mass and Topographic Change

Changes in ground surface height,  $z(x,y)$ , are described by the continuity of mass equation for a terrain surface, which is expressed in terms of the divergence of the sediment flux  $\mathbf{q}_s$  (dimensions of bulk volume rate per unit width):

$$\frac{\partial z}{\partial t} = -\nabla \mathbf{q}_s + U(x, y, t)$$

where  $z$  is surface height,  $t$  is time, and  $U$  is a source term that represents baselevel change or tectonic uplift. The first term on the right-hand side embodies several different sediment transport and erosion terms and can take on a number of different forms depending on the assumptions made about process mechanics. The formulations of the transport and erosion terms and the numerical solution to (1) are described below.

### 3.3 Spatial Framework

In order to avoid the limitations associated with grid-based models, the terrain surface may be discretized as a set of points (nodes) in any arbitrary configuration. These nodes are connected to form a triangulated irregular mesh (Figs. 1, 3) (Braun and Sambridge, 1997; Tucker et al., 2000). The mesh is constructed using the Delaunay triangulation, which is the (generally) unique set of triangles having the property that a circle passing through the three nodes of any triangle will contain no other nodes (e.g., Du, 1996). The use of an irregular spatial framework offers several significant advantages: (1) the model resolution can vary in space in order to represent certain landscape features, such as floodplains or regions of complex terrain, at a locally high level of detail (e.g., Fig. 1); (2) adaptive remeshing can be used to adjust spatial resolution dynamically in response to changes in the nature or rates of processes occurring at a particular location (e.g., Braun and Sambridge, 1997; Tucker et al., 2001; and examples below); (3) nodes can

be moved horizontally as well as vertically, making it possible to simulate lateral and surface-normal, as opposed to purely vertical, erosion (as, for example, in the cases of meandering channels and cliff retreat); (4) nodes can be added to simulate lateral accretion of, for example, point bars in meandering streams or accretionary wedges at active margins; and (5) the terrain can be coupled with 3D kinematic or dynamic models of tectonic deformation in order to simulate interactions between crustal deformation (e.g., shortening, fold growth) and topographic change. The data structures used to implement the triangular mesh are described by Tucker et al. (2001).

The Delaunay framework lends itself to a numerical solution of the continuity equation (Eq 1) using finite-volume methods. Each node (vertex) in the triangulation,  $N_i$ , is associated with a Voronoi (or Thiessen) polygon of surface area  $\Lambda_i$  (Fig. 3), in which the polygon edges are perpendicular bisectors of the edges connecting the node to its neighbors (e.g., Du, 1996; Guibas and Stolfi, 1986). Thus, the Delaunay triangulation defines the connectivity between adjacent nodes, while the associated Voronoi diagram defines the surface area associated with each node as well as the width of the interface between each pair of adjacent nodes (Fig. 3B). In CHILD, each Voronoi polygon is treated as a finite-volume cell. Continuity of mass for each node is written using an ordinary differential equation:

$$\frac{dz_i}{dt} = \frac{1}{\Lambda_i} \sum_{j=1}^{M_i} Q_{Sji} ,$$

where  $z_i$  is the average surface height of node  $i$ ,  $M_i$  is the number of neighbor nodes connected to node  $i$ , and  $Q_{Sji}$  is the total bulk volumetric sediment flux from node  $j$  to node  $i$  (negative if the net flux is from  $i$  to  $j$ ). Note that by this method it is only possible to describe the average rate of erosion or deposition within a given Voronoi polygon. As described below, the method used to integrate the flux terms depends on whether the flux is two-dimensional (e.g., for diffusive sediment transport or kinematic-wave overland flow routing) or one-dimensional (for streamwise water and sediment routing). For discussion of the implementation, application, and advantages of irregular discretization in landscape models, the reader is referred to Braun and Sambridge (1997) and Tucker et al. (2001).

### 3.4 Temporal Framework

One of the challenges in modeling terrain evolution lies in addressing the great disparity between the time scales of topographic change (e.g., years to geologic epochs) and the time scales of storms and floods (e.g., minutes to days). Most previous models of drainage basin evolution have dealt with this

disparity by simply assuming a constant average climatic input (e.g., a steady rainfall rate or a “geomorphically effective” runoff coefficient). This approach, while computationally efficient, has three drawbacks: (1) it ignores the influence of intrinsic climate variability on rates of erosion and sedimentation (e.g., Tucker and Bras, 2000); (2) it fails to account for the stochastic dynamics that arise when a spectrum of events of varying magnitude and frequency acts in the presence of geomorphic or hydrologic thresholds; and (3) the approach typically relies on a poorly calibrated “climate coefficient” that cannot be directly related to measured climate data.

In order to surmount these limitations, and to address the role of event magnitude and frequency in drainage basin evolution, CHILD uses a stochastic method to represent rainfall variability. The method is described in detail by Tucker and Bras (2000), and is only briefly outlined here. In solving the continuity equation, the model iterates through a series of alternating storms and interstorm periods, based on the Poisson rainfall model developed by Eagleson (1978). Each storm event is associated with a constant rainfall intensity,  $P$ , a duration,  $T_r$ , and an inter-arrival “waiting time”,  $T_b$  (Fig. 4). For each storm, these three attributes are chosen at random from exponential probability distributions, the parameters for which can be readily derived from hourly rainfall data (Eagleson, 1978; Hawk, 1992). Alternatively, storm intensity, duration, and frequency may be kept constant, in which case the approach reduces to the “effective rainfall intensity” approximation (Tucker and Slingerland, 1997). In either case, storms are approximated as having constant intensity throughout their duration, and the same assumption is also applied to the resulting hydrographs. Runoff-driven transport and erosion processes (described below) are computed only during storm events. Other processes, including diffusive creep transport and tectonic deformation, are assumed to occur continuously, and are updated at the end of each interstorm period (Fig. 5).

Note that the model imposes no special restrictions on time scale, aside from the fact that it is designed for periods longer than the duration of a single storm. For simulations involving terrain evolution over thousands to millions of years (e.g., Tucker and Slingerland, 1997), however, it becomes computationally intractable to simulate individual storms. For many applications this problem can be overcome by simply amplifying the storm and interstorm durations. As long as the ratio  $T_r/T_b$  remains the same, the underlying frequency distributions are preserved. Perturbations in climate can also be simulated by changing the parameters of the three frequency distributions (Fig. 4).

### 3.4.1 Stochastic Rainfall: Example

Figure 6 illustrates the behavior of the model under stochastic rainfall forcing, in a case where a high erosion threshold (see below) lends the system a high sensitivity to extreme events. The initial condition consists of a 30 degree slope upon which are superimposed small random perturbations in the elevation of each node. Erosion of the slope in response to a random series of rainfall and runoff events (Fig. 6A) is highly episodic (Fig. 6B). In this example, a gully forms early on in response to a series of large-magnitude and relatively long-duration storms (Figs. 6C and E). The gully develops in an area where the topography of the initial surface leads to local flow convergence. The reduction in gradient along the gully effectively stabilizes the system, so that later events have little or no impact. Subsequent mass movement by slope-driven diffusive creep (see below) leads to gradual healing of the scar (Figs. 6D and F).

## 3.5 Surface Hydrology and Runoff Generation

Surface runoff collected at each node on the mesh is routed downslope toward one of its adjacent neighbor nodes, following the edge that has the steepest downhill slope (Fig. 3). If a closed depression occurs on the mesh, water can either be assumed to evaporate at that point, or alternatively a lake-filling algorithm can be invoked to find an outlet for the closed depression (Tucker et al., 2000).

The local contribution to runoff at a node is equal to the effective runoff rate (defined below) multiplied by the node's Voronoi area,  $\Lambda$ . The drainage area,  $A$ , at a node is the sum of the area of all Voronoi cells that contribute flow to that node. Total surface discharge can be computed from drainage area using one of three methods. The first two assume that runoff generation is spatially uniform, while the third represents variable-source area runoff generation.

### 3.5.1 Hortonian (infiltration-excess) runoff

Runoff production (rainfall rate minus infiltration rate) is assumed to be uniform across the landscape. Assuming steady-state flow, the surface discharge at any point is equal to

$$Q = (P - I_c)A, \quad P > I_c,$$

where  $I_c$  is infiltration capacity (L/T).



### 3.5.2 Excess storage capacity runoff

Under this approach, the soil, canopy, and surface are collectively assumed to have a finite and spatially uniform capacity to absorb rainfall. Any rainfall exceeding this storage depth will contribute to runoff according to

$$R = \frac{T_r P - D_{sr}}{T_r}, \quad T_r P > D_{sr}$$

where  $R$  is local runoff rate (L/T),  $D_{sr}$  is the soil-canopy-surface retention depth (L), and the resulting discharge at any point is  $Q = RA$ . Note that equation (4) describes a runoff rate that is constant throughout a storm and equal to the total volume of excess rainfall divided by the storm duration. Note also that  $R = 0$  if  $D_{sr} > T_r P$ .

### 3.5.3 Saturation-excess runoff

With this option, a modified form of O'Loughlin's (1986) topographically based method is used to partition rainfall between overland and shallow subsurface flow. The capacity for shallow subsurface flow per unit contour length ( $q_{sub}$ ) is assumed to depend on local slope ( $S$ ) and soil transmissivity ( $T$ , dimensions of  $L^2/T$ ),

$$q_{sub} = \frac{Q_{sub}}{w} = TS$$

where contour length is represented by the width of adjoining Voronoi cell edges,  $w$ . The surface flow component is equal to the total discharge minus the amount that travels in the subsurface,

$$Q = PA - TS w, \quad PA > TS w.$$

Here,  $Q$  represents surface discharge resulting from a combination of saturation-excess overland flow and return flow. Note that this method assumes hydrologic steady state for both surface and subsurface flows, and thus is most applicable to prolonged storm events and/or highly permeable shallow soils.

### 3.5.4 Example

The mechanism of runoff production can impact both terrain morphology and dynamic responses to changing climate, land-use, or tectonism. For example, theoretical studies have shown that the mode of runoff production can have a significant impact on terrain morphology, drainage density, and the scaling of drainage density with relief and climate (Kirkby, 1987; Ijjasz-Vasquez et al., 1992; Tucker and Bras, 1998). Figure 7 compares two simulated drainage basins formed under Hortonian and saturation-excess runoff production, respectively. All other parameters in the two simulations are identical. In the saturation case, runoff is rarely generated on hillslopes. As a result, hillslopes are steep and highly convex (reflecting the dominance of diffusive creep-type sediment transport; see below). The difference is reflected in slope-area plots for the two simulated basins. In the case of the saturation-dominated basin, the hillslope-channel break is well described by the line of saturation for the mean-intensity storm (Fig. 7D).

## 3.6 Hillslope Mass Transport

Sediment transport by “continuous” hillslope processes such as soil creep is modeled using the well-known hillslope diffusion equation (e.g., Culling, 1960; McKean et al., 1993),

$$\left. \frac{\partial z}{\partial t} \right|_{\text{creep}} = -\nabla(-k_d \nabla z) = k_d \nabla^2 z,$$

where  $k_d$  is a transport coefficient with dimensions of  $L^2/T$ . Numerical solution to equation (7) is obtained using a finite-volume approach (Tucker et al., 2000). The net mass flux for a node is taken as the sum of the mass fluxes through each face of its Voronoi polygon (Eq (2)). For each pair of adjacent nodes, the gradient across their shared Voronoi polygon edge is approximated as the gradient between the nodes themselves. The total flux between each pair of nodes is thus equal to the topographic gradient between them multiplied by the width of their shared Voronoi edge, so that Eq (7) is approximated numerically as

$$\left. \frac{\partial z_i}{\partial t} \right|_{\text{creep}} = -\frac{k_d}{\Lambda_i} \sum_{j=1}^{M_i} S_{ij} w_{ij},$$

where  $S_{ij} = (z_i - z_j)/\lambda_{ij}$  is the downslope gradient from node  $i$  to node  $j$ ,  $\lambda_{ij}$  is the distance between  $i$  and  $j$  (i.e., the length of the triangle edge connecting them), and  $w_{ij}$  is the width of the shared Voronoi polygon face (Fig. 3B).

For steeper gradients, a nonlinear form of Eq (7) is arguably more appropriate to describe the effects of accelerated creep and intermittent landsliding (e.g., Anderson and Humphrey, 1990; Roering et al., 1999). Although this type of nonlinear rate law is not presently coded in CHILD, its incorporation would be straightforward.

Note also that equation (7) is intended to model creep-type processes rather than wash erosion. Instead, wash and channel erosion are effectively lumped together under the same formulation, as described below. This approach has the obvious disadvantage that wash is effectively treated as a form of rill erosion in which rills have the same hydraulic geometry (i.e., width, depth, and roughness properties) as larger channels, with all the attendant limitations this implies. On the other hand, lumping rill and channel erosion in a single “runoff erosion” category has the advantage of simplicity: no extra parameters are needed to differentiate between hillslopes and channels (as is the case, for example, in the model of Willgoose et al., 1991a), which emerge solely as a result of process competition (Kirby, 1994; Tucker and Bras, 1998). Thus, while we acknowledge a need for a more rigorous sub-model for wash erosion in the future, the treatment of wash as a general form of channel erosion seems justified given the aims of the model and the present uncertainty regarding the dynamics of channel initiation.

### 3.7 Water Erosion and Sediment Transport

At each node, the local rate of water erosion is equal to the lesser of (1) the detachment capacity, or (2) the excess sediment transport capacity. Both of these are represented as power functions of slope and discharge, and they are assumed to be mutually independent. Deposition occurs where sediment flux exceeds transport capacity (for example, due to a downstream reduction in gradient). The maximum detachment capacity depends on local slope and discharge according to

$$D_c = k_b \left( k_t \left( \frac{Q}{W} \right)^{m_b} S^{n_b} - \theta_{cb} \right)^{p_b},$$

where  $D_c$  is the maximum detachment (erosion) capacity (L/T),  $W$  is channel width,  $\theta_{cb}$  is a threshold for particle detachment (e.g., critical shear stress), and  $k_b$ ,  $k_t$ ,  $m_b$ ,  $n_b$ , and  $p_b$  are parameters. Note that with suitably

chosen parameters, equation (9) can represent either excess shear stress (i.e.,  $\tau$  = bed shear stress,  $\tau_{cb}$  = critical shear stress for detachment) or excess stream power (Whipple and Tucker, 1999). The shear stress formulation is similar to that used in the drainage basin evolution models of Howard (1994) and Tucker and Slingerland (1997), as well as a number of soil erosion models (e.g., Foster and Meyer, 1972; Mitas and Mitasova, 1998). If the Manning equation is used to model roughness,  $m_b=0.6$ ,  $n_b=0.7$ , and  $k_r=\rho g n^{3/5}$ , where  $\rho$  is water density,  $g$  is gravitational acceleration, and  $n$  is Manning's roughness coefficient. If the Chezy equation is used,  $m_b=2/3$ ,  $n_b=2/3$ , and  $k_r=\rho g C^{1/2}$ , where  $C$  is the Chezy roughness coefficient (for derivations, see Tucker and Slingerland, 1997; Whipple and Tucker, 1999).

Channel width is computed empirically, using the well-known scaling relationships between channel width and discharge (Leopold and Maddock, 1958; Leopold et al., 1964):

$$W = W_b (Q / Q_b)^{\omega_s}, W_b = k_w Q_b^{\omega_b}$$

where  $W_b$  is bankfull channel width,  $Q_b$  is a characteristic discharge (such as bankfull or mean annual),  $k_w$  is bankfull width per unit scaled discharge, and  $\omega_b$  and  $\omega_s$  are the downstream and at-a-station scaling exponents, respectively. Although these laws were developed for alluvial streams, they appear to be applicable to other fluvial systems (e.g., Ibbitt, 1997) such as steep mountain channels (Snyder et al., 2000).

The transport capacity for detached sediment material of a single grain size is based on a generalization of common bedload and total-load sediment transport formulas, which are typically expressed as a function of excess shear stress or stream power (e.g., Yang, 1996). For steady, uniform flow in a wide channel,

$$C_s = W k_f \left( k_t \left( \frac{Q}{W} \right)^{m_f} S^{n_f} - \theta_c \right)^{p_f},$$

where  $C_s$  is transport capacity ( $L^3/T$ ) and  $k_f$ ,  $k_t$ ,  $m_f$ ,  $n_f$ , and  $p_f$  are parameters. As with equation (9), equation (11) can be expressed in terms of excess shear stress or stream power using suitably chosen values for  $k_t$ ,  $m_f$ , and  $n_f$ . For transport of multiple sediment size-fractions, an alternative approach based on the method of Wilcock (1997, 1998) is used (this is described below).

Three end-member cases can arise from equations (9) and (11): detachment-limited behavior, transport-limited behavior, and mixed-channel behavior:

1. *Detachment-limited*: If the sediment transport capacity is everywhere much larger than the rate of sediment supply, the rate of water erosion is simply equal to the maximum detachment rate,

$$\frac{\partial z_b}{\partial t} = -D_c,$$

where  $z_b$  represents elevation of the channel bed above a datum within the underlying rock column. This type of formulation has been used in a number of studies to represent bedrock channel erosion (or more generally, detachment-limited erosion of cohesive, cemented, or non-granular materials) (e.g., Howard and Kerby, 1983; Seidl and Dietrich, 1992; Anderson, 1994; Howard et al., 1994; Moglen and Bras, 1995; Sinclair and Ball, 1996; Stock and Montgomery, 1999; Whipple and Tucker, 1999; Snyder et al., 2000). An important assumption is that the sediment flux has no direct control on the rate of incision, as long as there is sufficient capacity to transport the eroded material (cf. Sklar and Dietrich, 1998). Note that this case has the practical advantage of being efficient to solve numerically. Though widely used, however, the accuracy of this approximation for long-term stream profile development remains to be evaluated.

2. *Transport-limited*: If sufficient sediment is always available for transport and/or the bed material is easily detached (i.e., high  $k_b$ ), streams are assumed to be everywhere at their carrying capacity. Under this condition, continuity of mass gives the local rate of erosion or deposition as

$$\frac{\partial z_b}{\partial t} = -\frac{1}{(1-\nu)} \frac{\partial C_s / W}{\partial \mathbf{x}},$$

where  $\nu$  is bed sediment porosity (usually absorbed into the transport coefficient  $k_p$ ) and  $\mathbf{x}$  is a vector oriented in the direction of flow. Transport-limited behavior has been assumed in a number of models (e.g., Snow and Slingerland, 1987; Willgoose et al., 1991a; Tucker and Bras, 1998; Gasparini et al., 1999), though its applicability to bedrock streams has been questioned (e.g., Howard et al., 1994).

3. *Mixed-channel systems*: The detachment and transport formulas imply a third category of behavior that arises under conditions of (1) active erosion into resistant material (e.g., bedrock) and (2) high sediment supply. Under these conditions, active detachment of bed material must occur (by definition), but the sediment supply rates are sufficiently high that the local rate of incision is limited by the excess transport capacity (e.g., Tucker and Slingerland, 1996). Stream channels falling into this category might be

expected to have (on average) a partial cover of alluvium over bedrock; we thus refer to streams falling into this category as mixed-channel systems (Howard, 1998). Under certain conditions, the transition point between one type of behavior (e.g. detachment-limited) and another (e.g. mixed) can be computed analytically. Mixed channel behavior is discussed in greater depth by Whipple and Tucker (in review).

### 3.7.1 Example

In the special case of a constant rate of surface lowering, equations (12) and (13) both imply a power-law relationship between channel gradient and contributing area (Willgoose et al., 1991b; Howard, 1994; Whipple and Tucker, 1999), which is consistent with river basin data (e.g., Hack, 1957; Flint, 1974). Figure 8 shows an example of such scaling for two simulated landscapes. The straight lines indicate the trend that would occur under purely transport-limited conditions (solid line; e.g., Willgoose et al., 1991b) and under purely detachment-limited conditions (dashed line; e.g., Howard, 1994). Theoretical considerations suggest that longitudinal profile concavity, which is indicated by the slope of the lines on Figure 8, should generally be lower in transport-limited alluvial channels (Howard, 1994). The intersection of the two lines indicates the point at which the gradient required to transport eroded sediment becomes equal to the gradient required to detach particles. Upstream of this point, channel gradient is dictated by detachment capacity; downstream, the channel falls into the “mixed” category in which active incision occurs but the gradient is controlled by sediment supply. Under constant runoff, the transition point is abrupt (Fig. 8A), but in the more realistic case of variable flows, the transition is gradational and spread over two or more orders of magnitude in drainage area (Fig. 8B). This result implies that such detachment-to-transport transitions, even if they do exist, would be very difficult to identify on the basis of morphology alone (this of course excludes channel-type transitions that are forced by tectonic or other controls).

## 3.8 Extension to Multiple Grain Sizes

Size-selective erosion, transport, and deposition are important as agents that control the texture of alluvial deposits. Textural properties of ancient strata are important not only for the information they reveal about the geologic past (e.g., Paola et al., 1992; Robinson and Slingerland, 1998), but also for their control on the movement and storage of water and hydrocarbon resources (e.g., Koltermann and Gorelick, 1992). Perhaps surprisingly, recent work has also shown that the dynamics of size-selective erosion and

transport can have a significant impact on drainage basin architecture and evolution (Gasparini, 1998; Gasparini et al., 1999). Size-selective sediment transport and armoring can also exert important controls on the erosional history of artificial landforms such as mine tailing heaps, and are therefore important for engineering applications (Willgoose and Riley, 1998).

To model size-selective erosion and deposition, CHILD uses a two-fraction (sand and gravel) approach based on the bedload entrainment and transport functions developed by Wilcock (1997, 1998). The rock or sediment column underlying each node in the model contains a mixture of sand and gravel sediment fractions. An active layer of depth  $L_{act}$  defines the depth over which sediment near the surface is well mixed and accessible for active erosion and deposition (Gasparini, 1998; Gasparini et al., 1999). The transport capacities of the two size fractions are given by

$$q_{sg} = \frac{C_w f_g}{(s-1)g} \left( \frac{\tau}{\rho} \right)^{1.5} \left[ 1 - \frac{\tau_{cg}}{\tau} \right]^{4.5}$$

$$q_{ss} = \frac{C_w f_s}{(s-1)g} \left( \frac{\tau}{\rho} \right)^{1.5} \left[ 1 - \sqrt{\frac{\tau_{cs}}{\tau}} \right]^{4.5}$$

where  $q_{sg}$  and  $q_{ss}$  are the transport rates of gravel and sand, respectively (kg/ms),  $C_w$  is a dimensionless constant equal to 11.2,  $f_g$  and  $f_s$  are the fractions of gravel and sand in the bed,  $\rho$  is water density,  $s$  is the ratio of sediment and water density,  $g$  is gravitational acceleration,  $\tau$  is bed shear stress, and  $\tau_{cg}$  and  $\tau_{cs}$  are the critical shear stresses needed to entrain gravel and sand, respectively.

Wilcock (1997; 1998) analyzed the relative mobility of sand and gravel fractions in gravel-sand mixtures, and found that the initiation of motion threshold for both fractions approaches a constant (and minimum) value for mixtures containing more than about 40% sand. The threshold of motion criterion criteria used in CHILD's gravel-sand transport module is based on a piecewise linear fit to the data of Wilcock (1997) (Gasparini et al., 1999).

The active layer represents the depth over which active particle exchange takes place. For modeling instantaneous transport, the active layer is typically defined on the basis of grain diameter. For modeling average transport rates over the duration of one or many floods, this definition is inappropriate, because local scour and the movement of bars and bedforms

allow the flow to access significantly more near-bed sediment than simply the uppermost one or two grain diameters. Paola and Seal (1995) suggested that bankfull channel depth might be an appropriate choice for active layer thickness for calculating long-term average transport rates. However, in the absence of data on what controls the “effective mixing depth” over a given time period, we adopt here the simple approach of using an active layer of constant thickness. Sensitivity experiments by Gasparini (1998), which show little variation in equilibrium texture patterns with varying active layer depth, provide some justification for this approach, though we acknowledge a need for deeper understanding of this issue.

Detachment of cohesive or intact sediment is assumed to be size-independent and governed by Eq (9). When the multiple grain-size option is used, detached material is assumed to break down into a user-specified proportion of gravel and sand, which is then subject to differential entrainment and transport according to Eqs (14) and (15).

### 3.9 Deposition and Stratigraphy

There has been an increasing recognition of the importance of coupling between erosional and depositional systems (e.g., Humphrey and Heller, 1995; Johnson and Beaumont, 1995; Tucker and Slingerland, 1996; Densmore et al., 1998). An important goal behind developing CHILD has been to create a system that can be used to investigate these interactions and their role in shaping the terrestrial sedimentary record. For this reason, CHILD includes a “layering” module that records depositional stratigraphy.

Each node in the model is underlain by a column of material divided into a series of layers of variable thickness and properties. Physical attributes associated with each layer include the relative sand and gravel fractions (if applicable), the median grain size of each sediment fraction, and the material detachability coefficient,  $k_b$ . These properties are assumed to be homogeneous within a given layer. The time of most recent deposition is also stored for each layer, so that chronostratigraphy can be simulated. Finally, each layer also records the amount of time it has spent exposed at the surface, which is useful for identifying periods of quiescence and may be applicable to modeling exposure-age patterns in conjunction with cosmogenic isotope studies.

The active layer depth is fixed in time and space. When material is eroded from the surface, the active layer is replenished with material from the layer below. The active layer texture and time of surface exposure are then updated as a weighted average between the current properties of the active layer and those of the layer below. Bedrock is never mixed into sediment layers. When there are no sediment layers below the surface, the



active layer is depleted until no sediment remains and the channel is on bedrock. During deposition, material from the active layer is moved into the layer below before material is deposited into the active layer, so that the active layer depth remains constant. The layers below the active layer have a maximum depth; when this depth will be exceeded due to deposition, a new layer is created.

### 3.9.1 Example

Fault-bounded mountain ranges and alluvial fans in regions of tectonic extension are classic examples of close coupling between erosional and depositional systems (e.g., Leeder and Jackson, 1993; Ellis et al., 1999). Alluvial fan stratigraphy is shaped by a combination of forces, including extrinsic factors such as tectonic uplift/subsidence and climate change, and intrinsic factors related to the dynamics and geometry of sediment erosion, transport, and deposition. Numerical modeling of these systems can be used to evaluate the feasibility of conceptual models, to explore their sensitivity to external controls, and to suggest new hypotheses regarding the stratigraphic and geomorphic signatures of tectonic and climatic change.

Figure 9 shows a simple example of a simulated mountain range bounded by an alluvial fan complex. In this example, we have chosen a simple experimental design in which a block consisting of a cohesionless sand-gravel mixture rises vertically at a constant rate relative to an adjacent (fixed) basin surface and its associated baselevel. As one might expect, the simulation shows a set of alluvial fans that prograde across the basin surface (Fig. 9). A “wave” of sand-rich sediment progrades ahead of the advancing fan toes (Figs. 9A, B). Interestingly, size-selective transport occurs not only within the fan complex but also within the source terrain. Initially, finer material is removed from the surface of the rising block, leaving behind a coarsened layer of surface sediment that rims the headward-encroaching drainages. Thus, the grain-size patterns within the fan complex are influenced in part by sorting within the source terrain. Whether this effect occurs in nature must depend on the regolith thickness; while bare rock slopes offer little opportunity for grain-size fractionation, such fractionation has been observed to occur on soil-mantled, wash-dominated slopes (e.g., Abrahams and Parsons, 1991).

Note that in this example no attempt is made to simulate either downstream flow branching or sheetflow; rather, flow is effectively spread across the fan surface through time as channels shift in response to depositional patterns. A transverse section across the fan complex (Fig. 10) reveals that the main fan bodies are, perhaps counter-intuitively, slightly

finer than the inter-fan areas. This behavior would have implications for fluid reservoir modeling, as it implies that in some cases inter-fan areas may have locally higher hydraulic conductivity.

### 3.10 Lateral Stream Channel Migration (Meandering)

Owing to the large difference in scale between individual stream channels and their drainage basins, channels are generally treated as one-dimensional entities in landscape evolution theory. For many applications, this choice is entirely appropriate; for others, however, it is problematic because it neglects the role of floodplains as sediment buffers (e.g., Trimble, 1999). This limitation is particularly severe in analyses of watershed responses to perturbations (e.g., Tucker and Slingerland, 1997). At the same time, the morpho-stratigraphic development of floodplains is an important problem in its own right (e.g., Mackey and Bridge, 1995; Moody et al., 1999). These issues have motivated the development of a simple “rules based” model of channel meandering, based on the principle of topographic steering, which is capable of modeling channel planform evolution on time scales relevant to valley, floodplain, and stream terrace development (Lancaster, 1998; Lancaster and Bras, in press).

Lateral channel migration is implemented in CHILD by first identifying main channel (meandering) nodes on the basis of a drainage area threshold. Lateral migration of these nodes occurs perpendicular to the downstream direction, and the rate is proportional to the bank shear stress:

$$\hat{\zeta} = E_{eff} \tau_w \hat{n}$$

where  $\hat{\zeta}$  is the migration vector of the outer bank,  $\tau_w$  is the bank shear stress determined by the meandering model of Lancaster and Bras (in press; see also Lancaster, 1998);  $\hat{n}$  is the unit vector perpendicular to the downstream direction; and  $E_{eff}$  is the effective bank erodibility, defined by:

$$E_{eff} = E_0 \left( \frac{1 - P_H h_B}{H + h_B} \right), \quad h_B > 0, \\ = E_0, \quad h_B \leq 0$$

where  $E_0$  is the nominal bank erodibility;  $H$  is water depth;  $h_B$  is bank height above the water surface; and  $P_H$  is the degree to which the effective bank erodibility is dependent on bank height, where  $0 \leq P_H \leq 1$  (Lancaster, 1998). This bank height dependence directly couples topography and

migration rate. Each channel node in the model actually has both right and left bank erodibilities, and these values are determined from a weighted average of  $E_{\text{eff}}$  values calculated for neighboring nodes falling on either side of the line perpendicular to the downstream direction (Fig. 11). We write the effective erodibility at node  $i$  of the bank on the  $\hat{e}$ -side as

$$E_{\text{eff},i}^{(\hat{e})} = \frac{E_{\text{eff},i1}d_2 + E_{\text{eff},i2}d_1}{d_1 + d_2}$$

where  $\hat{e}$  is the unit vector in the direction of either the left ( $\hat{n}$ ) or right ( $-\hat{n}$ ) bank;  $E_{\text{eff},i1}$  and  $E_{\text{eff},i2}$  are the effective erodibilities of the bank nodes with respect to node  $i$ ; and  $d_1$  and  $d_2$  are the distances of the bank nodes from the line parallel to the unit vector,  $\hat{e}$  (Fig. 11).

We use the meandering model of Lancaster (1998) to find  $\tau_w$  in (16) as a function of channel curvature upstream. Movement of a channel node indicates that the channel centerline has moved, i.e., that one bank has been eroded while deposition has occurred at the other. As the channel migrates, existing nodes are deleted from the moving channel's path, and new nodes are added in the moving channel's wake. Node movement and addition require re-determination of node stratigraphy.

A flow chart in Figure 12 illustrates the implementation of meandering within the CHILD model. The discretization of meandering channel reaches is dependent on channel width and is, in general, different from the discretization of the surrounding landscape. This procedure is described in more detail in Lancaster (1998).

### 3.10.1 Examples

An example simulation incorporating the stream meander model is shown in Figure 13. Here the model is configured to represent an idealized segment of floodplain, with a large stream (point source of discharge) entering at the top of the mesh and exiting at the bottom. The hydrology and initial topography are patterned after Wildcat Creek, a 190 km<sup>2</sup> drainage basin in north-central Kansas. In this example, the mainstream elevation is forced with a series of cut-fill cycles (representing millennial-scale climate impacts), while the stream planform is free to migrate laterally. Each point along the main channel is moveable. Dynamic remeshing is used to ensure that the mainstream is adequately resolved. Whenever a moving channel point comes very close to a fixed "bank" point, the latter is removed from the mesh. To ensure an adequate level of spatial resolution within the floodplain, a new point is added in the "wake" of a moving channel point

whenever the moving point has migrated a given distance away from a previously stored earlier location (which is then updated). The net result is that the floodplain is modeled at a locally high resolution relative to the surrounding uplands (Fig. 13).

A similar approach can be used to investigate the development of incised meanders in bedrock such as those of the Colorado Plateau (e.g., Gardner, 1975) and the Ozark Mountains. Lancaster (1998) modeled the development of terrain under active uplift, incision, and stream meandering, and found that coupling between bank height and the rate of cut-bank erosion exerts an important influence on the resultant topography and channel planforms.

### 3.11 Floodplains: Overbank Sedimentation

Valley-fill sediments often contain an important record of paleoclimate, paleo-geomorphology, and prehistory (e.g., Johnson and Logan, 1990). Most studies of the formation and dynamics of river basins have treated streams as essentially one-dimensional conduits of mass and energy. Yet valley-fill sediments are inherently three-dimensional features, and to model their stratigraphy properly requires an alternative approach. The one-dimensional approach cannot, for example, resolve important aspects of alluvial stratigraphy such as the distribution of channel and overbank deposits (e.g., Mackey and Bridge, 1995). Motivated by this limitation, CHILD includes the capability to model overbank sedimentation using a modified form of Howard's (1992) floodplain diffusion model. Under this approach, the rate of overbank sedimentation during a flood varies as a function of distance from a primary channel and local floodplain topography. Average rates of floodplain sedimentation are known to decay with distance from the source channel due to diffusion of turbulent energy. The local rate of sedimentation is also presumed to depend on the height of the floodplain relative to water surface height. During a given storm event, the rate of overbank sedimentation at a given point is

$$D_{OB} = (\eta - z)\mu \exp(-d / \lambda)$$

where  $D_{OB}$  is the vertical deposition rate (dimensions of L/T),  $z$  is local elevation,  $d$  is the distance between the point in question and the nearest point on the main channel,  $\eta$  is the water surface height at the nearest point on the main channel,  $\mu$  is a deposition rate constant ( $T^{-1}$ ), and  $\lambda$  is a distance-decay constant. "Main channel" is defined on the basis of a drainage area threshold; typically, the model would be configured with a large channel fed in as a boundary condition for this type of application, so that there would be no ambiguity about what constitutes a primary channel (e.g., Fig. 13). Water

surface height is computed as the sum of bed elevation,  $z$ , and water depth,  $H$ , using a simple empirical hydraulic geometry approach for  $H$ :

$$H = H_b (Q / Q_b)^{\delta_s}, \quad H_b = k_w Q_b^{\delta_b}$$

where  $H_b$  is bankfull channel depth,  $Q_b$  is a characteristic discharge (such as bankfull or mean annual),  $k_w$  is bankfull depth per unit scaled discharge, and  $\delta_b$  and  $\delta_s$  are the downstream and at-a-station scaling exponents, respectively (Leopold et al., 1964). Equation (19) is only applied for events in which  $H > H_b$ .

### 3.11.1 Example

Combining channel meandering and overbank deposition makes it possible to simulate the development of three-dimensional alluvial stratigraphic architecture, which has been the goal of a number of different models (e.g., Howard, 1992; Mackey and Bridge, 1995; Teles et al., 1998). The fill terraces depicted in Figure 13 are formed during times of rising baselevel along the main channel. Lateral channel migration etches out the fills during intervals of cutting. Inset terraces are formed during subsequent fill episodes (Fig. 13). Among other things, this type of stratigraphic simulation can provide a basis for developing and testing improved geostatistical methods for modeling 3D subsurface architecture (e.g., de Marsily et al., 1998).

## 4. DISCUSSION: APPLICATIONS AND LIMITATIONS

All models involve a tradeoff between simplicity and realism. What makes the CHILD model unique is its ability to examine interactions among a wide range of processes, in scenarios that range from simple to complex. The examples herein use simple, idealized scenarios to illustrate these processes. The model's design reflects the fundamental recognition that the characteristics of one part of a river basin are determined in large part by the characteristics of the basin upstream and, to a lesser degree, downstream.

The inclusion of many process modules and alternative parameterizations in one model (Fig. 2) is intended to enhance the researcher's ability to address very simple and well-posed questions by carefully selecting a subset of process equations and configuring these with appropriate initial and boundary conditions. By comparing model behavior under varying levels of

complexity and/or different process models, the validity and robustness of different simplifying assumptions can be tested. One can examine, for example, the consequences of relaxing the common assumption of homogeneous sediment size (Gasparini et al., 1999), or assess the appropriateness of using a “characteristic storm” parameter as a surrogate for time-varying rainfall and flood discharge (Tucker and Bras, 2000).

CHILD has been developed as a framework for modeling changes in drainage basin terrain over a range of space and time scales. Although there are no explicit limits to spatial scale, the assumption of hydrologic steady state during storm events is most valid for relatively small watersheds (less than perhaps  $100\text{km}^2$ ), in which the time of concentration is shorter than the duration of a typical storm. Similarly, the assumption of spatially uniform precipitation rate, infiltration capacity and soil transmissivity is only appropriate for small watersheds (although one might also wish to make similar assumptions in simple “what if” studies of large-scale landscape evolution). At the lower end of spatial scales, the approximation of steady, uniform unidirectional flow loses validity for the length scales on which momentum and backwater effects become important (on the order of decimeters to meters). The assumption of steady rainfall and runoff during storms also implies that the model is most applicable to time periods much longer than the duration of a single storm. The upper limit to time scale is dictated only by performance considerations, and in fact for certain applications it is feasible to magnify storm and interstorm durations to enhance computational speed.

Distributed models necessarily involve a tradeoff between speed and resolution. The CHILD model’s TIN-based framework offers an advantage in this regard, because it makes it possible to vary spatial resolution as a function of dominant process or landscape position (Figs. 1 and 13). On the other hand, the use of variable spatial resolution complicates the inclusion of “scale-dependent physics” (i.e., equations whose rate constants depend on spatial scale). This may be a blessing in disguise, for although it makes the problem of calibration in engineering applications more difficult it also provides a disincentive to scale-dependent “tuning” of parameters. Use of a variable-resolution numerical mesh, if handled properly, may also help resolve certain scaling issues that arise as a result of averaging terrain properties over an arbitrary and fixed discretization scale. For example, with an irregular discretization method it becomes possible (at least in principle) to construct a discretized terrain surface that uses the minimum necessary number of computational points to accurately represent hillslope gradient at all points in a region of complex terrain. The TIN framework also opens the door to bridging the two fundamental and disparate scales in watershed hydrology, that of the channel and that of the basin as a whole.

Although it is intended to serve a wide range of applications, the CHILD model's roots lie in large-scale drainage basin morphology and evolution. The form of many of the equations used in CHILD reflects this emphasis. Thus, the sediment transport equations are based on formulas commonly used to predict bedload transport rates, and the model at this stage includes no explicit treatment of suspended or wash load (which are presumably of lesser importance in controlling stream gradients). Similarly, the model at present includes no expressions for landsliding or for eolian transport. The emphasis on physical rather than chemical process renders CHILD inapplicable in solution-dominated environments (e.g., karst terrain). It should be emphasized, however, that CHILD is designed with extensibility in mind, and the modular design of the software reflects this (Tucker et al., 2001). Recent efforts to adapt CHILD for applications in forestry (Lancaster et al., 1999) and flood hydrology (Rybarczyk et al., 2000) demonstrate the utility of constructing modular and extensible numerical modeling systems.

There is no simple answer to the question of how to test and validate a model such as CHILD because it is in essence not one model but many, each with different assumptions, aims, and requirements. Ultimately, the basis for validation or rejection of a model should depend on the nature of the problem addressed. Nonetheless, it is worth noting that several methods for evaluating the predictions of landscape evolution theory have been advanced recently. Statistical approaches have been widely used to examine drainage network properties (e.g., Rodriguez-Iturbe and Rinaldo, 1997), although some network statistics suffer from a lack of discriminant ability (e.g., Kirchner, 1993). Experimental approaches have also been used (Hancock and Willgoose, in review). Arguably the most promising tests of landscape evolution theory come from settings in which paleo-topography (e.g., Stock and Montgomery, 1998) and driving factors such as uplift rate (e.g., Merritts and Vincent, 1989; Snyder et al., 2000) are independently known. Much can be learned by testing the morphologic predictions of landscape evolution models against observed terrain in regions where some type of equilibrium is believed to exist (e.g., Willgoose, 1994). The CHILD model, as with other models based on similar fluvial erosion formulations, can successfully reproduce theoretically predicted slope-area scaling under conditions of spatially uniform erosion rate (a form of equilibrium). This simply reflects the fact that the exponent terms in the fluvial transport and erosion terms can be chosen such that the model-predicted scaling under either equilibrium (uplift-erosion balance) or transient decline agrees with observed values (e.g., Willgoose et al., 1991a; Howard, 1994; Willgoose, 1994; Whipple and Tucker, 1999; Tucker and Whipple, in review). However, one disadvantage of testing models on the basis of equilibrium states, aside from the difficulty

in establishing the existence of such states in the first place, is the potential for equifinality (i.e., different processes may lead to the same outcome, as in the case of slope-area scaling discussed by Tucker and Whipple, in review).

Landscapes characterized by a transient response to a known perturbation contain useful information about process dynamics that is often lost in equilibrium states (Tucker and Whipple, in review; Whipple and Tucker, in review). Hence, one of the key research needs is to identify transient landscapes in which knowledge of the nature and timing of the causative external perturbation, whether of tectonic, climatic, geomorphic, or human origin, can be obtained. For short-term phenomena such as gully development, there is a need for detailed monitoring to establish time sequences of landform development.

## 5. SUMMARY AND CONCLUSIONS

CHILD is a new computer model of drainage basin evolution that integrates a wide variety of processes, many of which have not been included in previous models of drainage basin evolution. The model is designed to serve as a general-purpose framework for investigating a range of issues in drainage basin geomorphology, with an emphasis on morphological development. Some components of the model, such as the treatment of channel and hillslope erosion, use an approach similar to that of existing models. The model also includes a number of new features and capabilities that are designed to foster the development of theoretical geomorphology by making it possible to investigate in greater detail the feedbacks between hillslope/channel hydrology and landscape evolution, and to examine coupling between erosional and depositional systems. The incorporation of (1) meandering and (2) floodplain deposition, which have not before been included in models of drainage basin evolution, makes it possible to investigate the development of alluvial stratigraphy in the drainage basin context. Other capabilities, which are unique in their combination, include (3) stochastic storm variability, with an explicit link to climate data; (4) both detachment- and transport-limited fluvial erosion, with transport of either single- or dual-size sediment; (5) explicit tracking of subsurface stratigraphy, including time of deposition, textural properties, and deposit exposure ages; (6) variable, triangulated discretization and adaptive remeshing, which allow detailed resolution of particular features and representation of horizontal surface motion; and (7) infiltration-, storage- and saturation-excess runoff mechanisms, the last of which provides a direct link between topography and hydrology. Other capabilities, including a dynamic vegetation component



(Tucker et al., 1999) and kinematic thrust-fault propagation, are under development and will be described elsewhere.

To implement these capabilities, CHILD includes several process “modules.” In some cases, these represent alternative models for the same process (e.g., Hortonian versus saturation-excess runoff generation). Although the number of parameters in the model is potentially quite large, the many different capabilities and process equations are in fact developed with simplicity and flexibility in mind. CHILD’s extensible design facilitates the process of comparing alternative process models and conducting sensitivity experiments that address the basic (and important) questions of “what matters and when.”

Although developed with an emphasis on research applications, CHILD’s more detailed treatment of hydrology also makes it well suited to potential applications in land management and erosion prediction. Most soil erosion models, such as USLE and WEPP, assume a one-dimensional and unchanging topography. These limitations, though appropriate for estimating soil loss under rill and interrill erosion, are poorly suited to modeling gully and channel incision, phenomena in which dynamic modification of landforms and flow aggregation play a central role.

## Acknowledgments

This research was supported by the U.S. Army Corps of Engineers Construction Engineering Research Laboratories (USACERL), the U.S. Army Research Office, and the Italian National Research Council. We are grateful to Lainie Levick for a helpful review, and to William Doe and Russell Harmon for convening the workshop and GSA Special Session that led to this volume.

## REFERENCES

- Abrahams, A.D., and Parsons, A.J., 1991, Relation between sediment yield and gradient on debris-covered hillslopes, Walnut Gulch, Arizona: Geological Society of America Bulletin, v. 103, p. 1109-1113.
- Ahnert, F., 1970, A comparison of theoretical slope models with slopes in the field: Zeitschrift fur Geomorphologie, v. 9, p. 88-101.
- Ahnert, F., 1976, Brief description of a comprehensive three-dimensional process-response model of landform development: Zeitschrift fur Geomorphologie, v. 25, 29-49.
- Anderson, R.S., 1994, Evolution of the Santa Cruz Mountains, California, through tectonic growth and geomorphic decay: Journal of Geophysical Research, v. 99, p. 20,161-20,179.

- Anderson, R.S., and Humphrey, N.F., 1990, Interaction of weathering and transport processes in the evolution of arid landscapes, in Cross, T., ed., *Quantitative dynamic stratigraphy*: Englewood Cliffs, N.J., Prentice-Hall p. 349-361.
- Armstrong, A.C., 1976, A three-dimensional simulation of slope forms: in *Quantitative Slope Models*, ed. by F. Ahnert, *Zeitschrift fur Geomorphologie*, Supplement Band 25, p. 20-28.
- Beaumont, C., Fullsack, P., and Hamilton, J., 1992, Erosional control of active compressional orogens, in McClay, K.R., ed., *Thrust tectonics*: New York, Chapman and Hall, p. 1-18.
- Braun, J., and Sambridge, M., 1997, Modelling landscape evolution on geological time scales: a new method based on irregular spatial discretization: *Basin Research*, v. 9, p. 27-52.
- Chase, C.G., 1992, Fluvial landsculpting and the fractal dimension of topography: *Geomorphology*, v. 5, p. 39-57.
- Coulthard, T.J., Kirkby, M.J., and Macklin, Mark G., 1997, Modelling the impacts of Holocene environmental change in an upland river catchment, using a cellular automaton approach, in Brown, A.G., and Quine, T.A., eds., *Fluvial processes and environmental change*, British Geomorphological Research Group symposia series, p. 31-46.
- Culling, W.E.H., 1960, Analytical theory of erosion: *Journal of Geology*, v. 68, p. 336-344.
- Densmore, A.L., Ellis, M.A., and Anderson, R.S., 1998, Landsliding and the evolution of normal-fault-bounded mountains: *Journal of Geophysical Research*, v. 103, p. 15,203-15,219.
- Du, C., 1996, An algorithm for automatic Delaunay triangulation of arbitrary planar domains: *Advances in Engineering Software*, v. 27, p. 21-26.
- Eagleson, P.S., 1978, Climate, soil, and vegetation: 2. the distribution of annual precipitation derived from observed storm sequences: *Water Resources Research*, v. 14, p. 713-721.
- Ellis, M.A., Densmore, A.L., and Anderson, R.S., 1999, Development of mountainous topography in the Basin Ranges, USA: *Basin Research*, v. 11, p. 21-41.
- Favis-Mortlock, D., 1998, A self-organizing dynamic systems approach to the simulation of rill initiation and development of hillslopes: *Computers & Geosciences*, 24 (4), p. 353-372.
- Flint, J.J., 1974, Stream gradient as a function of order, magnitude, and discharge: *Water Resources Research*, v. 10, p. 969-973.
- Foster, G.R., and Meyer, L.D., 1972, A closed-form erosion equation for upland areas, in Shen, H.W., ed., *Sedimentation: Symposium to Honor Professor H. A. Einstein*, p. 12.1-12.19, Colorado State University, Fort Collins, CO.
- Gardner, T.W., 1975, The history of part of the Colorado River and its tributaries; an experimental study, *Field Symposium - Guidebook of the Four Corners Geological Society* (8), p. 87-95.
- Gasparini, N.M., 1998, *Erosion and Deposition of Multiple Grain Sizes in a Landscape Evolution Model*, unpublished M.Sc. thesis, Massachusetts Institute of Technology.
- Gasparini, N.M., Tucker, G.E., and Bras, R.L., 1999, Downstream fining through selective particle sorting in an equilibrium drainage network: *Geology*, v. 27, no. 12, p. 1079-1082.
- Gilbert, G.K., 1877, *Report on the geology of the Henry Mountains*: U.S. Geographical and Geological Survey of the Rocky Mountain Region, Washington, D.C., U.S. Government Printing
- Gossman, H., 1976, Slope modelling with changing boundary conditions---effects of climate and lithology: *Zeitschrift fur Geomorphologie*, v. 25, p. 72-88.
- Guibas, L., and Stolfi, J., 1985, Primitives for the manipulation of general subdivisions and the computation of Voronoi diagrams: *ACM Transactions on Graphics*, v. 4, no. 2, p. 74-123.
- Hack, J.T., 1957, *Studies of longitudinal stream profiles in Virginia and Maryland*: U.S. Geological Survey Professional Paper no. 294-B, 97 pp.

- Hancock, G., and Willgoose, G., in review, The use of a landscape simulator in the validation of the SIBERIA catchment evolution model: declining equilibrium landforms: Water Resources Research, submitted.
- Hawk, K.L., 1992, Climatology of station storm rainfall in the continental United States: parameters of the Bartlett-Lewis and Poisson rectangular pulses models, unpublished M.S. thesis, Department of Civil and Environmental Engineering, Massachusetts Institute of Technology, 330pp.
- Howard, A.D., 1992, Modeling channel and floodplain sedimentation in meandering streams, in *Lowland Floodplain Rivers: Geomorphological Perspectives*, John Wiley & Sons, Chichester, United Kingdom, p. 1-41.
- Howard, A.D., 1994, A detachment-limited model of drainage basin evolution: Water Resources Research, v. 30, p. 2261-2285.
- Howard, A.D., 1998, Long profile development of bedrock channels; interaction of weathering, mass wasting, bed erosion, and sediment transport, in Tinkler, Keith J., and Wohl, Ellen E. (editors), *Rivers over rock; fluvial processes in bedrock channels*, Geophysical Monograph, 107, p. 297-319
- Howard, A.D., Dietrich, W.E., and Seidl, M.A., 1994, Modeling fluvial erosion on regional to continental scales: *Journal of Geophysical Research*, v. 99, p. 13,971-13,986.
- Howard, A.D., and Kerby, G., 1983, Channel changes in badlands: *Geological Society of America Bulletin*, v. 94, p. 739-752.
- Humphrey, N.F., and Heller, P.L., 1995, Natural oscillations in coupled geomorphic systems: an alternative origin for cyclic sedimentation: *Geology*, v. 23, p. 499-502.
- Ibbitt, R.P., Evaluation of optimal channel network and river basin heterogeneity concepts using measured flow and channel properties, *J. Hydrol.*, 196, 119-138, 1997.
- Ijjasz-Vasquez, E.J., Bras, R.L., and Moglen, G.E., 1992, Sensitivity of a basin evolution model to the nature of runoff production and to initial conditions: *Water Resources Research*, v. 28, p. 2733-2741.
- Johnson, D.D., and Beaumont, C., 1995, Preliminary results from a planform kinematic model of orogen evolution, surface processes and the development of clastic foreland basin stratigraphy, in Dorobek, S.L., and Ross, G.M., eds., *Stratigraphic Evolution of Foreland Basins*, SEPM Special Publication 52, p. 3-24.
- Johnson, W.C., and Logan, 1990, Geoarchaeology of the Kansas River Basin, central Great Plains, in Lasca, N.P., and Donohue, J., eds., *Archaeological Geology of North America: Geological Society of America, Decade of North American Geology Centennial Special Volume 4*, p. 267-299.
- Kirchner, J.W. 1993, Statistical inevitability of Horton's laws and the apparent randomness of stream channel networks: *Geology (Boulder)*, 21 (7), p. 591-594.
- Kirkby, M.J., 1971, Hillslope process-response models based on the continuity equation: in *Slopes: form and process*, Institute of British Geographers Special Publication 3, p. 15-30.
- Kirkby, M.J., 1986, A two-dimensional simulation model for slope and stream evolution, in Abrahams, A.D., ed., *Hillslope processes*: Winchester, Mass., Allen and Unwin, p. 203-222.
- Kirkby, M.J., 1987, Modelling some influences of soil erosion, landslides and valley gradient on drainage density and hollow development: *Catena Supplement*, v. 10, p. 1-14.
- Koltermann, C.E., Gorelick, S.M., 1992, Paleoclimatic signature in terrestrial flood deposits, *Science*, 256 (5065), p. 1775-1782.
- Koons, P.O., 1989, The topographic evolution of collisional mountain belts: a numerical look at the Southern Alps, New Zealand, *American Journal of Science*, v. 289, p. 1041-1069.

- Lancaster, S.L., 1998, A nonlinear river meander model and its incorporation in a landscape evolution model, Ph.D. thesis, Massachusetts Institute of Technology.
- Lancaster, S.L., and Bras, R.L., 2000, A simple model of river meandering and its comparison to natural channels: Hydrologic Processes, in review.
- Lancaster, S.L., Hayes, S.K., and Grant, G.E., 1999, The interaction between trees and the landscape through debris flows: *Eos, Transactions AGU*, v. 80 (46), p. F425.
- Leeder, M.R., Jackson, J.A., 1993, The interaction between normal faulting and drainage in active extensional basins, with examples from the western United States and central Greece: *Basin Research*, 5 (2), p. 79-102.
- Leopold, L. and Maddock, T., 1953, The hydraulic geometry of stream channels and some physiographic implications: Professional Paper 252, United States Geological Survey.
- Leopold, L.B., Wolman, M.G., and Miller, J.P., 1964, *Fluvial processes in geomorphology*: New York, W.H. Freeman, 522 pp.
- Lifton, N.A., and Chase, C.G., 1992, Tectonic, climatic and lithologic influences on landscape fractal dimension and hypsometry: implications for landscape evolution in the San Gabriel Mountains, California: *Geomorphology*, v. 5, p. 77-114.
- Luke, J.C., 1972, Mathematical models of landform evolution: *Journal of Geophysical Research*, v. 77, p. 2460-2464.
- Mackey, S.D., and Bridge, J.S., 1995, Three-dimensional model of alluvial stratigraphy; theory and applications, *Journal of Sedimentary Research, Section B: Stratigraphy and Global Studies*, 65 (1), p. 7-31.
- Marsily, G. de, 1998, Some current methods to represent the heterogeneity of natural media in hydrogeology: *Hydrogeology Journal*, v. 6, p. 115-130.
- McKean, J.A., Dietrich, W.E., Finkel, R.C., Southon, J.R., and Caffee, M.W., 1993, Quantification of soil production and downslope creep rates from cosmogenic  $^{10}\text{Be}$  accumulations on a hillslope profile: *Geology*, v. 21, p. 343-346.
- Merritts, D., and Vincent, K.R., 1989, Geomorphic response of coastal streams to low, intermediate, and high rates of uplift, Mendocino junction region, northern California: *Geological Society of America Bulletin*, v. 101, p. 1373-1388.
- Mitas, L., and Mitasova, H., 1998, Distributed soil erosion simulation for effective erosion prevention: *Water Resources Research*, v. 34, p. 505-516.
- Moglen, G.E., and R.L. Bras, 1995, The Effect of Spatial Heterogeneities on Geomorphic Expression in a Model of Basin Evolution, *Water Resources Research* v. 31, no. 10, p. 2613-23.
- Moody, J.A., Pizzuto, J.E., and Meade, R.H., 1999, Ontogeny of a flood plain, *Geological Society of America Bulletin*, 111 (2), p. 291-303.
- O'Loughlin, E.M., 1986, Prediction of surface saturation zones in natural catchments: *Water Resources Research*, v. 22, p. 794-804.
- Penck, W., 1921, *Morphological analysis of land forms: a contribution to physical geography*: translated by Czech, H., and Boswell, K.C., London, Macmillan, 1953, 429 pp.
- Paola, C., Heller, P.L., and Angevine, C.L., 1992, The large-scale dynamics of grain-size variation in alluvial basins, 1: theory: *Basin Research*, v. 4, p. 73-90.
- Paola, C., and Seal, R., 1995, Grain size patchiness as a cause of selective deposition and downstream fining: *Water Resources Research*, v. 31, p. 1395-1407.
- Rigon, R., Rinaldo, A., and Rodriguez-Iturbe, I., 1994, On landscape self-organization: *Journal of Geophysical Research*, v. 99, p. 11,971-11,993.
- Robinson, Ruth A. J., Slingerland, Rudy L., 1998, Origin of fluvial grain-size trends in a foreland basin; the Pocono Formation on the central Appalachian Basin, *Journal of Sedimentary Research*, 68 (3), p. 473-486.

- Rodriguez Iturbe, I., and Rinaldo, A., 1997, Fractal river basins; chance and self-organization, 547 pp.
- Roering, J.J., Kirchner, J.W., and Dietrich, W.E., 1999, Evidence for nonlinear, diffusive sediment transport on hillslopes and implications for landscape morphology: *Water Resources Research*, v. 35, no. 3, p. 853-870.
- Rybarczyk, S.M., Ivanov, V.Y., Bras, R.L., and Tucker, G.E., 2000, Representing complex topography in distributed rainfall/runoff modeling: a TIN based approach, Paper presented at the International Francqui Chair Workshop on The Future of Distributed Hydrological Modelling, April 13th, Leuven, Belgium.
- Scheidegger, A.E., 1961, Mathematical models of slope development: *Geological Society of America Bulletin*, v. 72, p. 37-50.
- Seidl, M.A., and Dietrich, W.E., 1992, The problem of channel erosion into bedrock: *Catena Supplement* 23, p. 101-124.
- Sinclair, K., and Ball, R.C., 1996, Mechanism for global optimization of river networks for local erosion rules: *Physical Review Letters*, v. 76, p. 3360.
- Sinha, S.K., and Parker, G., 1996, Causes of concavity in longitudinal profiles of rivers: *Water Resources Research*, v. 32, p. 1417-1428.
- Sklar, L., and Dietrich, W.E., 1998, River longitudinal profiles and bedrock incision models; stream power and the influence of sediment supply, in Wohl, E., and Tinkler, K., *Rivers Over Rock: Fluvial Processes in Bedrock Channels*, AGU, Geophysical Monograph 107, p. 237-260.
- Smith, Terence R., Merchant, George E., 1995, Conservation principles and the initiation of channelized surface flows, in Costa, John E. (editor), Miller, Andrew J. (editor), Potter, Kenneth W. (editor), Wilcock, Peter R. (editor), *Natural and anthropogenic influences in fluvial geomorphology; the Wolman Volume*, Geophysical Monograph, 89, p. 1-25.
- Snow, R.S., and Slingerland, R.L., 1987, Mathematical modeling of graded river profiles: *Journal of Geology*, v. 95, p. 15-33.
- Snyder, N.P., Whipple, K.X., Tucker, G.E., and Merritts, D.J., 2000, Landscape response to tectonic forcing: DEM analysis of stream profiles in the Mendocino triple junction region, northern California: *Geological Society of America Bulletin*, in press.
- Stock, J., and Montgomery, D.R., 1999, Geologic constraints on bedrock river incision using the stream power law: *J. Geophys. Res.*, v. 104, p. 4983-4993.
- Teles, V., de Marsily, G., Perrier, E., 1998, Sur une nouvelle approche de modelisation de la mise en place des sediments dans une plaine alluviale pour en représenter l'heterogeneite: *C. R. Acad. Sci. Paris, Sciences de la Terre et des Planetes*, v. 327, p. 597-606.
- Trimble, S.W., 1999, Decreased rates of alluvial sediment storage in the Coon Creek basin, *Science*, 285 (5431), p. 1244-1246.
- Tucker, G.E., and Bras, R.L., 1998, Hillslope processes, drainage density, and landscape morphology: *Water Resources Research*, v. 34, p. 2751-2764.
- Tucker, G.E., and Bras, R.L., 2000, A stochastic approach to modeling the role of rainfall variability in drainage basin evolution: *Water Resources Research*, *Water Resources Research*, v. 36(7), pp. 1953-1964..
- Tucker, G.E., Gasparini, N.M., Bras, R.L., and Lancaster, S.L., 1999, A 3D Computer Simulation Model of Drainage Basin and Floodplain Evolution: Theory and Applications, Technical report prepared for U.S. Army Corps of Engineers Construction Engineering Research Laboratory.
- Tucker, G.E., Lancaster, S.T., Gasparini, N.M., Bras, R.L., and Rybarczyk, S.M., 2000, An object-oriented framework for distributed hydrologic and geomorphic modeling using triangulated irregular networks: *Computers and Geosciences*, in press.

- Tucker, G.E., and Slingerland, R.L., 1994, Erosional dynamics, flexural isostasy, and long-lived escarpments: a numerical modeling study: *Journal of Geophysical Research*, v. 99, p. 12,229-12,243.
- Tucker, G.E., and Slingerland, R.L., 1996, Predicting sediment flux from fold and thrust belts: *Basin Research*, v. 8, p. 329-349.
- Tucker, G.E., and Slingerland, R.L., 1997, Drainage basin responses to climate change: *Water Resources Research*, v. 33, no. 8, p. 2031-2047.
- Whipple, K.X., and Tucker, G.E., 1999, Dynamics of the stream power river incision model: implications for height limits of mountain ranges, landscape response timescales and research needs: *J. Geophys. Res.*, v. 104, p. 17,661-17,674.
- Wilcock, P., 1997, A method for predicting sediment transport in gravel-bed rivers: Technical report for the U.S. Forest Service Rocky Mountain Forest and Range Experiment Station, 59 pp.
- Wilcock, P., 1998, Two-fraction model of initial sediment motion in gravel-bed rivers: *Science*, v. 280, p. 410-412.
- Willgoose, G.R., 1994, A statistic for testing the elevation characteristics of landscape simulation models: *Journal of Geophysical Research*, v. 99, p. 13,987-13,996.
- Willgoose, G.R., Bras, R.L., and Rodriguez-Iturbe, I., 1991a, A physically based coupled network growth and hillslope evolution model, 1, theory: *Water Resources Research*, v. 27, p. 1671-1684.
- Willgoose, G.R., Bras, R.L., and Rodriguez-Iturbe, I., 1991b, A physical explanation of an observed link area-slope relationship: *Water Resources Research*, v. 27, p. 1697-1702.
- Willgoose, G.R., and Riley, S., 1998, The long-term stability of engineered landforms of the Ranger Uranium Mine, Northern Territory, Australia: Application of a catchment evolution model: *Earth Surface Processes and Landforms*, v. 23, p. 237-259.
- Yang, C.T., 1996, *Sediment transport: theory and practice*: New York, McGraw Hill, 396pp.

## FIGURE CAPTIONS

**Figure 1.** Example terrain simulations produced by CHILD. Thin solid lines are contours and heavy lines indicate drainage pathways. (A) simulation of gullying on an actual watershed (unnamed watershed on Fort Carson in the foothills of the Colorado Front Range near Colorado Springs). Inset shows a segment of the triangular mesh. (B) hypothetical fault-bounded mountain range. (C) valley and floodplain simulation, illustrating meandering stream with variable-resolution mesh. (D) rising mountain block with alluvial fans. Scales in (B), (D), and (D) are nominally 10 km, 1 km, and 2.5 km, respectively.

**Figure 2.** Components of the CHILD model.

**Figure 3.** Elements of the irregular computational mesh, showing nodes (solid circles), triangle edges (black lines), and Voronoi polygons (gray lines). Each Voronoi polygon acts as a finite volume cell. (A) streamflow is routed downslope from node to node along triangle edges, following the route of steepest descent. (B) two-dimensional diffusive exchange of sediment between node *N* and its neighbors. The diffusive mass flux per unit width between any two nodes is computed using the gradient between them. Multiplying unit flux by the width of their shared Voronoi polygon edge gives the total mass exchange rate.

**Figure 4.** Schematic illustration of Poisson rectangular pulse rainfall model (after Eagleson, 1978).

**Figure 5.** Flow chart illustrating the sequence of computations in CHILD.

**Figure 6.** Example of simulated gully erosion and healing in response to stochastic variations in rainfall intensity and duration. Here, a gully system forms and begins to heal on a planar slope (30 degrees, 100 by 100 meters) that is subjected to a series of random storm events. The landscape is highly sensitive to extreme events, owing to a large threshold for runoff erosion ( $\tau_c$ ) and a high soil erodibility coefficient ( $k_b$ ). (A) time series of rainfall events (durations not shown). (B) mean elevation of the surface through time, highlighting the episodic nature of denudation. Arrows indicate the times corresponding to plots C and D. (C) perspective plot of slope immediately after the last gully-forming episode. (D) perspective plot at the end of the simulation. (E) and (F) show contour plots at these two time slices. Equation set used in this run is  $-dz/dt = k_b(\tau - \tau_c)$  ( $k_b = 1.6 \times 10^{-5} \text{ m}^2 \text{ s kg}^{-1}$ ), with  $\tau = k_t(Q/W)^{2/3} S^{2/3}$  (Pa) ( $k_t = 6.2 \times 10^4 \text{ Pa s}^{2/3} \text{ m}^{-4/3}$ ),  $\tau_c = 20 \text{ Pa}$ , and  $W = 0.001 Q^{0.5}$  with  $Q$  in  $\text{m}^3/\text{s}$ . Rainfall parameters are  $\bar{P} = 0.64 \text{ mm/hr}$ ,  $\bar{T}_r = 32 \text{ hr}$ , and  $\bar{T}_b = 148 \text{ hr}$ ; hillslope diffusivity ( $k_d$ ) is  $0.01 \text{ m}^2/\text{yr}$ .

**Figure 7.** The influence of runoff-production mechanism on terrain morphology. (A) simulated drainage basin under infiltration-excess (Hortonian) runoff production (Eq (3)). (B) simulated basin under saturation-excess runoff production, using the O'Loughlin (1986) model (Eq (6)). (C), (D) plots of surface slope versus contributing area for the two cases. The line in (D) represents the line of saturation for the mean-intensity storm. In these examples runoff erosion is modeled as  $dz/dt \propto -Q^{0.5}S$ . Parameters are  $\bar{P} = 2.9 \text{ mm/hr}$ ,  $\bar{T}_r = 5 \text{ yr}$ ,  $\bar{T}_b = 95 \text{ yr}$ ,  $k_d = 0.01 \text{ m}^2/\text{yr}$ ,  $U = 0.1 \text{ mm/yr}$ , and in (B)  $T = 10^5 \text{ m}^2/\text{yr}$ .

**Figure 8.** Slope-area plots from two simulations illustrating a downstream transition from detachment-limited to transport-limited behavior under (A) constant runoff and (B) variable (stochastic) runoff. Both simulations are in equilibrium with a constant and spatially uniform rate of baselevel fall. The transport and erosion coefficients are adjusted so that the theoretical transition point occurs at the same drainage area in both cases. Although fluvial erosion theory predicts that such a transition should occur in many rivers, the result shown in (B) implies that transitions may be so smooth as to be undetectable in data.

**Figure 9.** Example of a simulated mountain-fan system, showing progradation of a set of alluvial fans in response to block uplift along a vertical fault. The substrate is treated as a cohesionless sediment pile containing a mixture of sand and gravel sediment fractions. Shading indicates the relative proportion of sand in the uppermost (active) sediment layer, with lighter shades indicating higher sand fraction. (A) 20,000 years after onset of uplift; (B) 40,000 years; (C) 100,000 years. Inset in (C) shows the location of cross-section in Figure 10. Uplift rate is  $1 \text{ mm/yr}$ , diffusivity is  $0.01 \text{ m}^2/\text{yr}$ , and rainfall parameters are  $\bar{P} = 1.1 \text{ mm/hr}$ ,  $\bar{T}_r = 3 \text{ yr}$ , and  $\bar{T}_b = 97 \text{ yr}$ .

**Figure 10.** Stratigraphic cross-section through the fan complex in Figure 9. Section is taken parallel to the strike of the range through the center of the fan complex (indicated by a-a' in Figure 9C). Black shading indicates less than 60% sand content.

**Figure 11.** Illustration of right bank ( $\hat{e} = -\hat{n}$ ) erodibility determination for node  $i$ .  $E_{\text{eff},i1}$  and  $E_{\text{eff},i2}$  are effective erodibilities with respect to node  $i$  at adjacent nodes that are distances  $d_1$  and  $d_2$ , respectively, from the line parallel to the unit vector,  $-\hat{n}$ . In the coordinate system shown, the  $s$ -direction is parallel to the flow edge, and the  $n$ -direction is perpendicular to the flow edge. Delaunay triangulation is in thin solid lines, Voronoi diagram is in dashed lines, and flow edges are in heavy black.

**Figure 12.** Flow chart showing the implementation of meandering.

**Figure 13.** Simulation of channel meandering and floodplain development. (A) perspective view of simulated topography, highlighting stream pattern and development of terraces (elevations are interpolated to regular grid for plotting purposes). (B) view of triangulated mesh, showing densification in the area of the floodplain (see text for details).



## Figure Captions

FIGURE 1. Examples of terrain simulations produced by CHILD. Thin solid lines are contours, heavy lines indicate drainage lines, and gray lines show the triangular computational mesh. (A) simulation of gullying on an actual watershed (unnamed watershed on Fort Carson in the foothills of the Colorado Front Range near Colorado Springs). (B) hypothetical fault-bounded mountain range. (C) valley and floodplain development, illustrating meandering stream with variable-resolution mesh. (D) rising mountain block and alluvial fans. Scales in (B), (D), and (D) are nominally 10 km, 1 km, and 2.5 km, respectively.

FIGURE 2. Overview of components in the CHILD model.

FIGURE 3. Elements of the irregular computational mesh, showing nodes (solid circles), triangle edges (black lines), and Voronoi polygons (gray lines). Each Voronoi polygon acts as a finite volume cell. (A) Streamflow is routed downslope from node to node along triangle edges, following the route of steepest descent. (B) Two-dimensional diffusive exchange of sediment between node  $N$  and its neighbors. The diffusive mass flux per unit width between any two nodes is computed using the gradient between them; multiplying by the width of their shared Voronoi polygon edge gives the total mass exchange rate.

FIGURE 4. Schematic illustration of Poisson rectangular pulse rainfall model (after Eagleson, 1978).

FIGURE 5. Flow chart illustrating the sequence of computations in CHILD.

FIGURE 6. Example of simulated gully erosion and healing in response to stochastic variations in rainfall intensity and duration. Here, a gully system forms and begins to heal on a planar slope (30 degrees, 100 by 100 meters) that is subjected to a series of random storm events. The landscape is highly sensitive to extreme events, owing to a large threshold for runoff erosion ( $\tau_c$ ) and a high soil erodibility coefficient ( $k_b$ ). (A) Time series of rainfall events (durations not shown). (B) Mean elevation of the surface through time, highlighting the episodic nature of denudation. Arrows indicate the times corresponding to plots C and D. (C) Perspective plot of slope immediately after the last gully-forming episode. (D) Perspective plot at the end of the simulation. (E) and (F) show contour plots at these two time slices. Equation set used in this run is  $-dz/dt = 505(\tau - \tau_c)$  (m/yr), with  $\tau = 0.62(Q/W)^{2/3}S^{2/3}$  (Pa),  $\tau_c = 20$  Pa, and  $W = 0.001 Q^{0.5}$  with  $Q$  in  $m^3/s$ . Rainfall parameters are  $\bar{P} = 0.64$  mm/hr,  $\bar{T}_r = 32$  hr, and  $\bar{T}_b = 148$  hr; hillslope diffusivity ( $k_d$ ) is  $0.01 m^2/yr$ .

FIGURE 7. The influence of runoff-production mechanism on terrain morphology. (A) Simulated drainage basin under infiltration-excess (Hortonian) runoff production (Eq (3)). (B) Simulated basin under saturation-excess runoff production, using the O'Loughlin (1986) model (Eq (6)). (C) and (D) plots of surface slope versus contributing area for the two cases. The line in (D) represents the line of saturation for the mean-intensity storm:  $S = (\bar{P}/(T_{w_v}))A$ . In these examples runoff erosion is modeled as  $-dz/dt = (1.44 \cdot 10^{-5})Q^{0.5}S$ . Other parameters are  $\bar{P} = 2.9$  mm/hr,  $\bar{T}_r = 5$  yr,  $\bar{T}_b = 95$  yr,  $k_d = 0.01 m^2/yr$ ,  $U = 0.1$  mm/yr, and in (B)  $T = 1.02 \cdot 10^5 m^2/yr$ .

FIGURE 8. Slope-area plots from two simulations illustrating a downstream transition from detachment-limited to transport-limited behavior under (A) constant runoff and (B) variable (stochastic) runoff. Both simulations are in equilibrium with a constant and spatially uniform rate of baselevel fall; the transport and erosion coefficients are adjusted so that the theoretical transition point occurs at the same drainage area in both cases. Although fluvial erosion theory predicts that such a transition should occur in many rivers, the result shown in (B) implies that transitions may be so smooth as to be undetectable in data.

FIGURE 9. Example of a simulated mountain-fan system, showing progradation of a set of alluvial fans in response to block uplift along a vertical fault. The substrate is treated as a cohesionless sediment pile containing a mixture of sand and gravel sediment fractions. Colors indicate the relative proportion of sand in the uppermost (active) sediment layer. (A) 20,000 years after onset of uplift; (B) 40,000 years; (C) 100,000 years. Inset in (C) shows the location of cross-sections in Figure 10. Uplift rate is 1 mm/yr, diffusivity is  $0.01 m^2/yr$ , and rainfall parameters are  $\bar{P} = 1.1$  mm/hr,  $\bar{T}_r = 3$  yr, and  $\bar{T}_b = 97$  yr.

FIGURE 10. Stratigraphic cross-sections through the fan complex in Figure 9. Sections A-C are taken normal to the strike of the range through the center of the fan complex (indicated by a-a' in Figure 9C) (note differences in vertical scales in A, B, C). Color scale for A-C is the same as in Figure 9. (D) shows transverse section at 1 km from the basin edge (b-b' in Figure 9C inset).

FIGURE 11. Illustration of right bank ( $\hat{e} = -\hat{n}$ ) erodibility determination for node  $i$ .  $E_{eff,i1}$  and  $E_{eff,i2}$  are effective erodibilities with respect to node  $i$  at adjacent nodes that are distances,  $d_1$  and  $d_2$ , respectively, from the line parallel to the unit vector,  $-\hat{n}$ . In the coordinate system shown, the  $s$ -direction is parallel to the flow edge, and the  $n$ -direction is perpendicular to the flow edge. Delaunay triangulation is in thin solid lines; Voronoi diagram is in dashed lines; and flow edges are in heavy black.

FIGURE 12. Flow chart showing the implementation of meandering.

FIGURE 13. Simulation of channel meandering and floodplain development. (A) Perspective view of simulated topography, highlighting stream pattern and development of terraces. (Elevations are interpolated to regular grid for plotting purposes). (B) View of triangulated mesh, showing densification in the area of the floodplain. (See text for details).

Figure 1

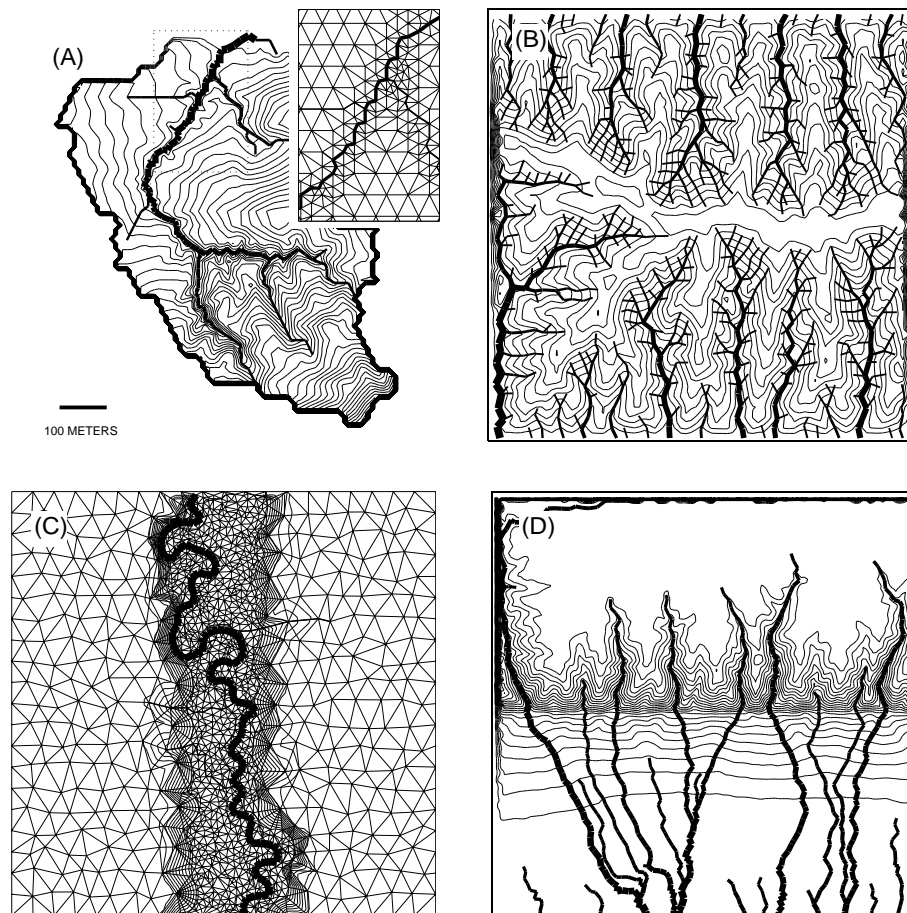


Figure 2

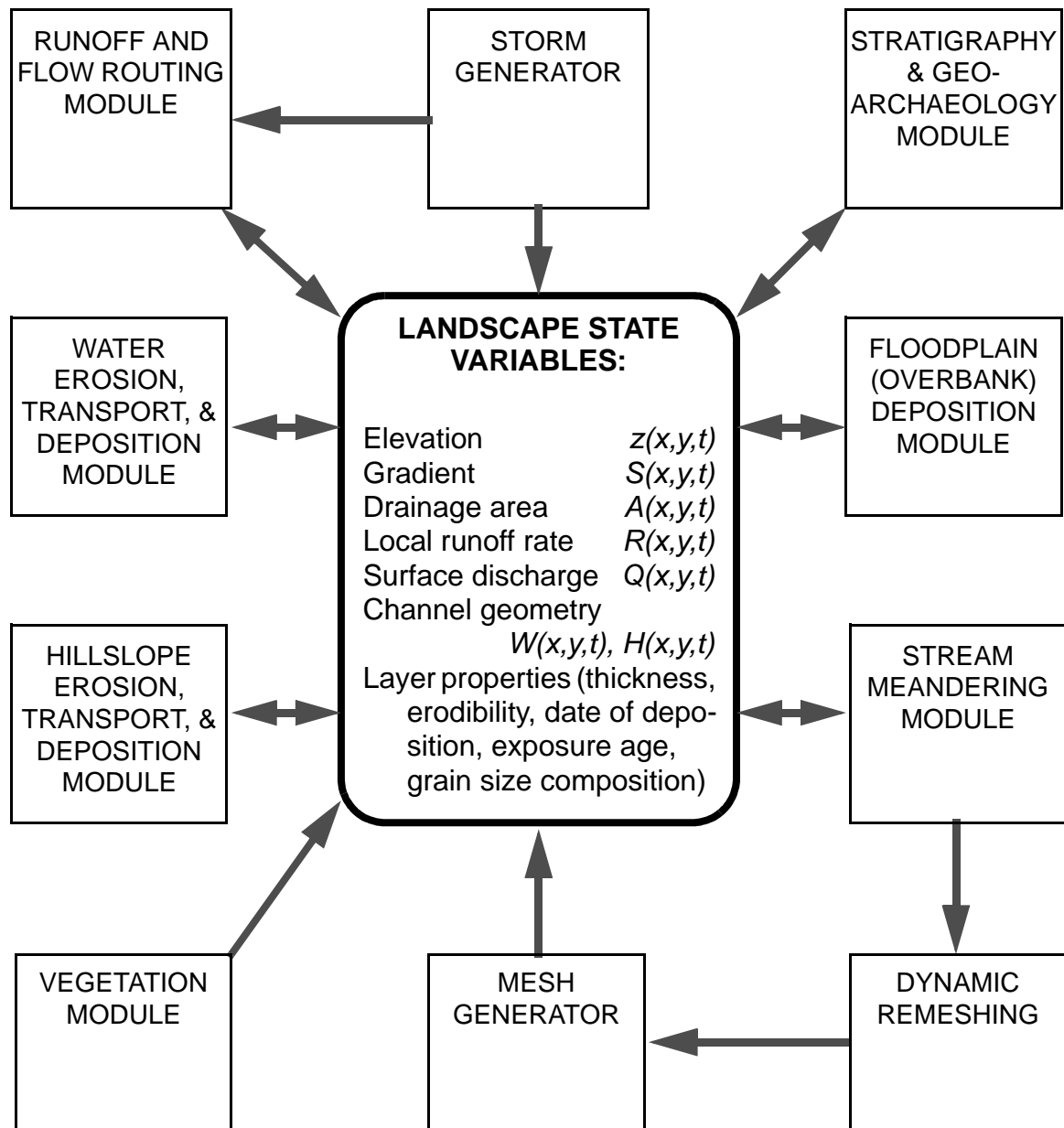


Figure 3

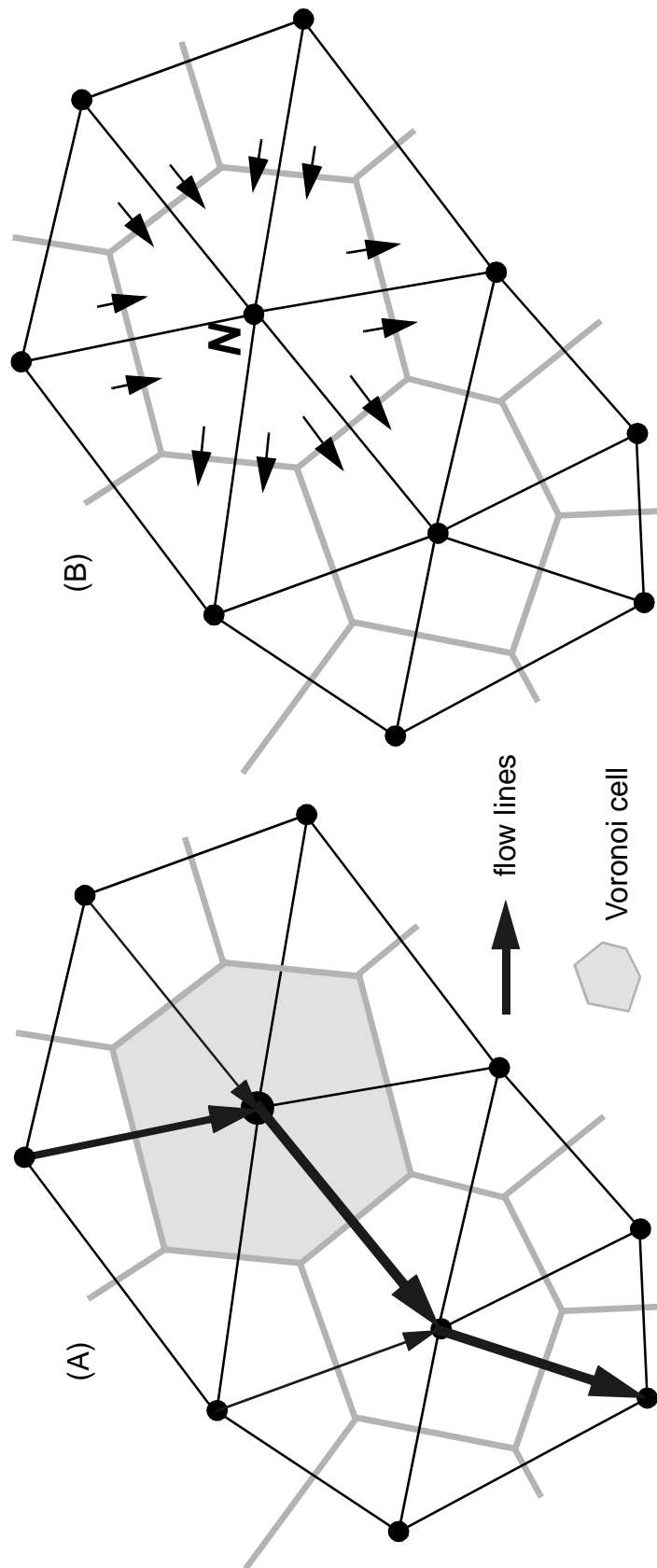


Figure 4

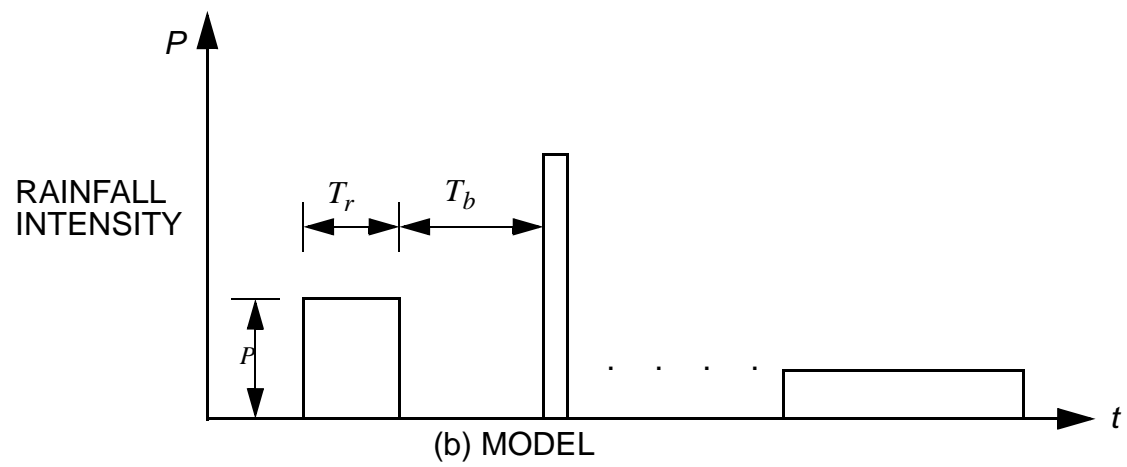
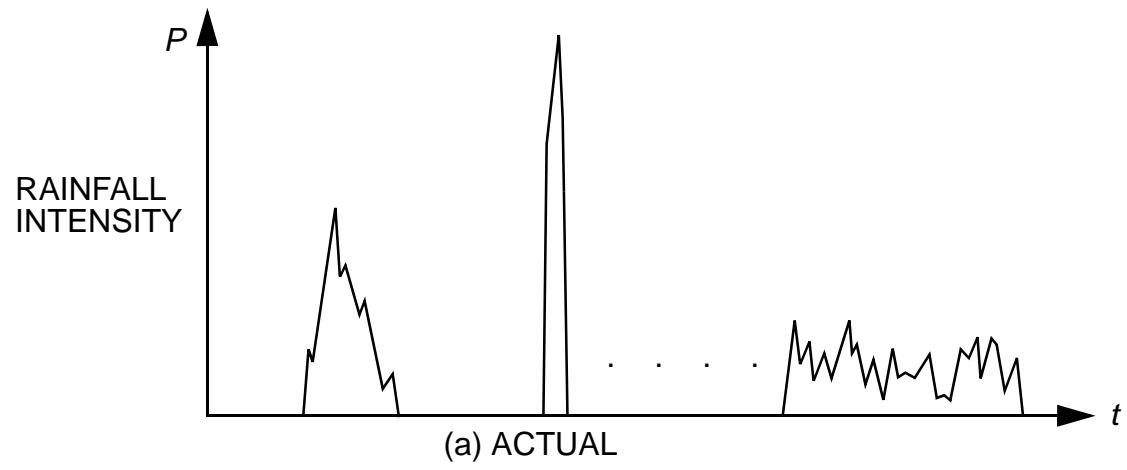


Figure 5

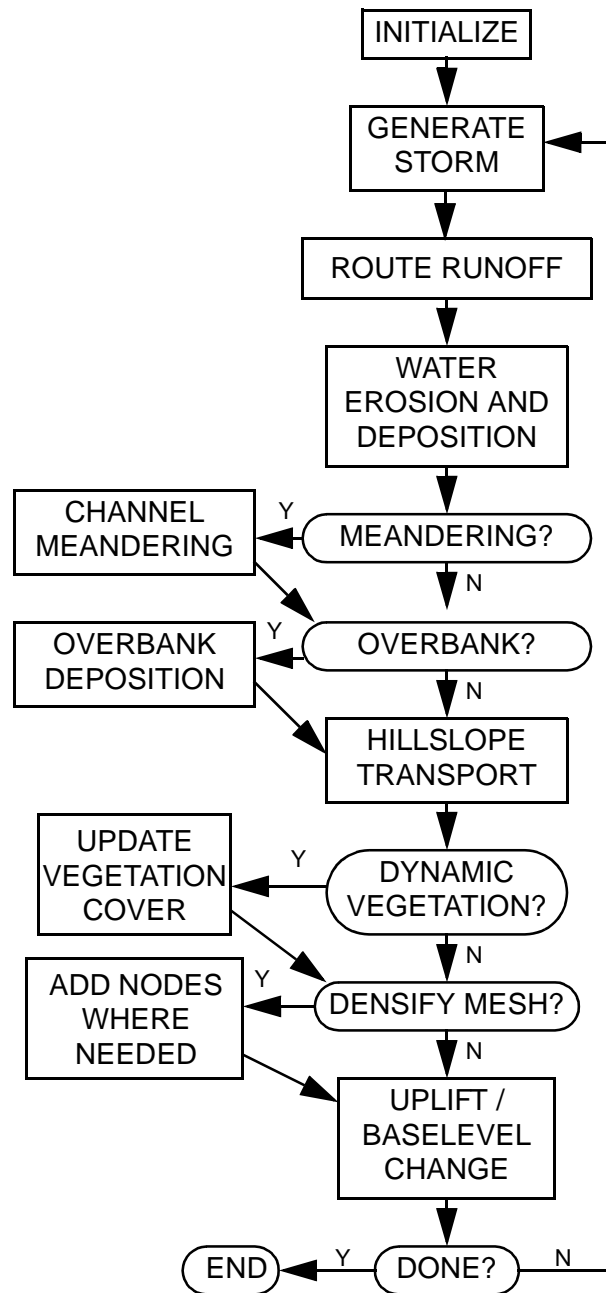


Figure 6

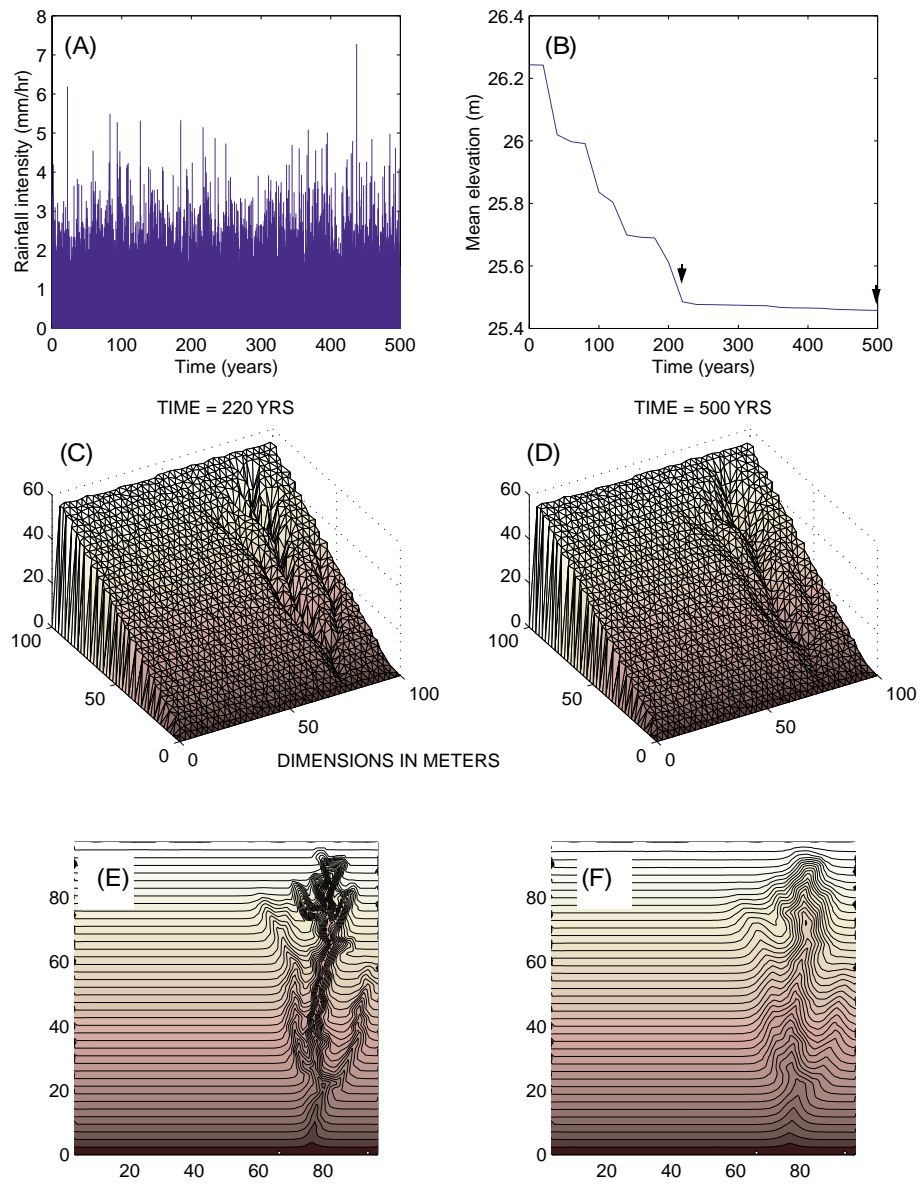




Figure 7

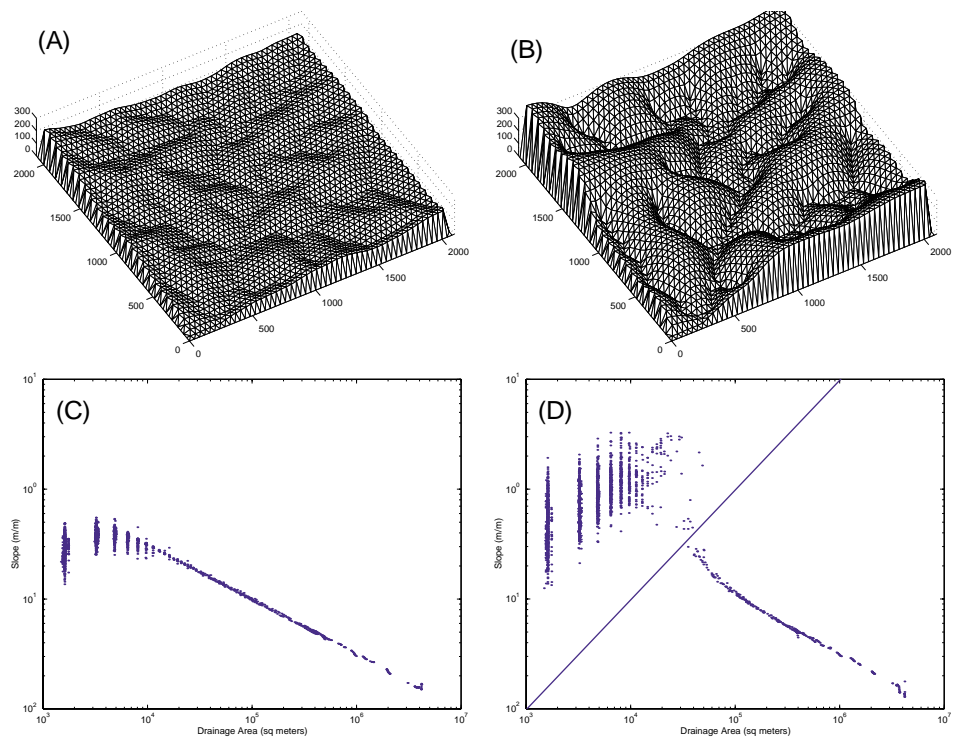


Figure 8

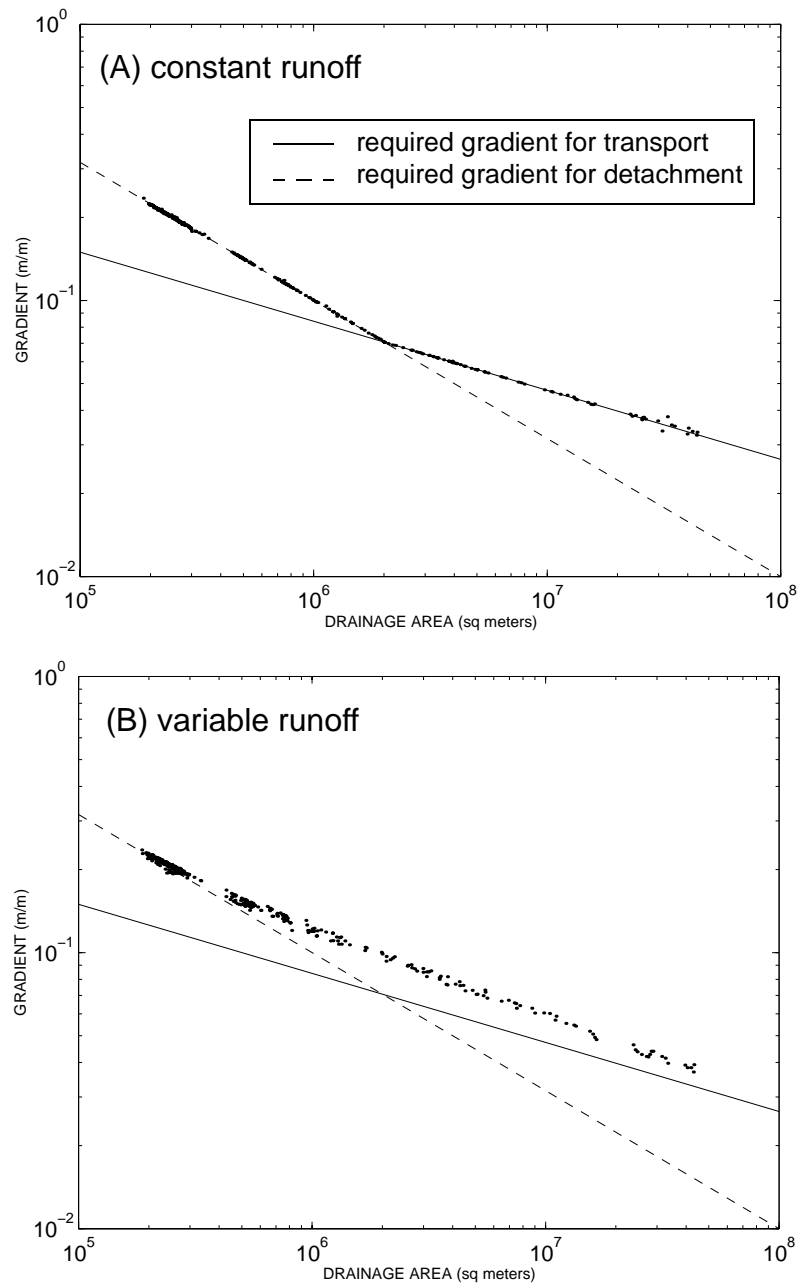


Figure 9a

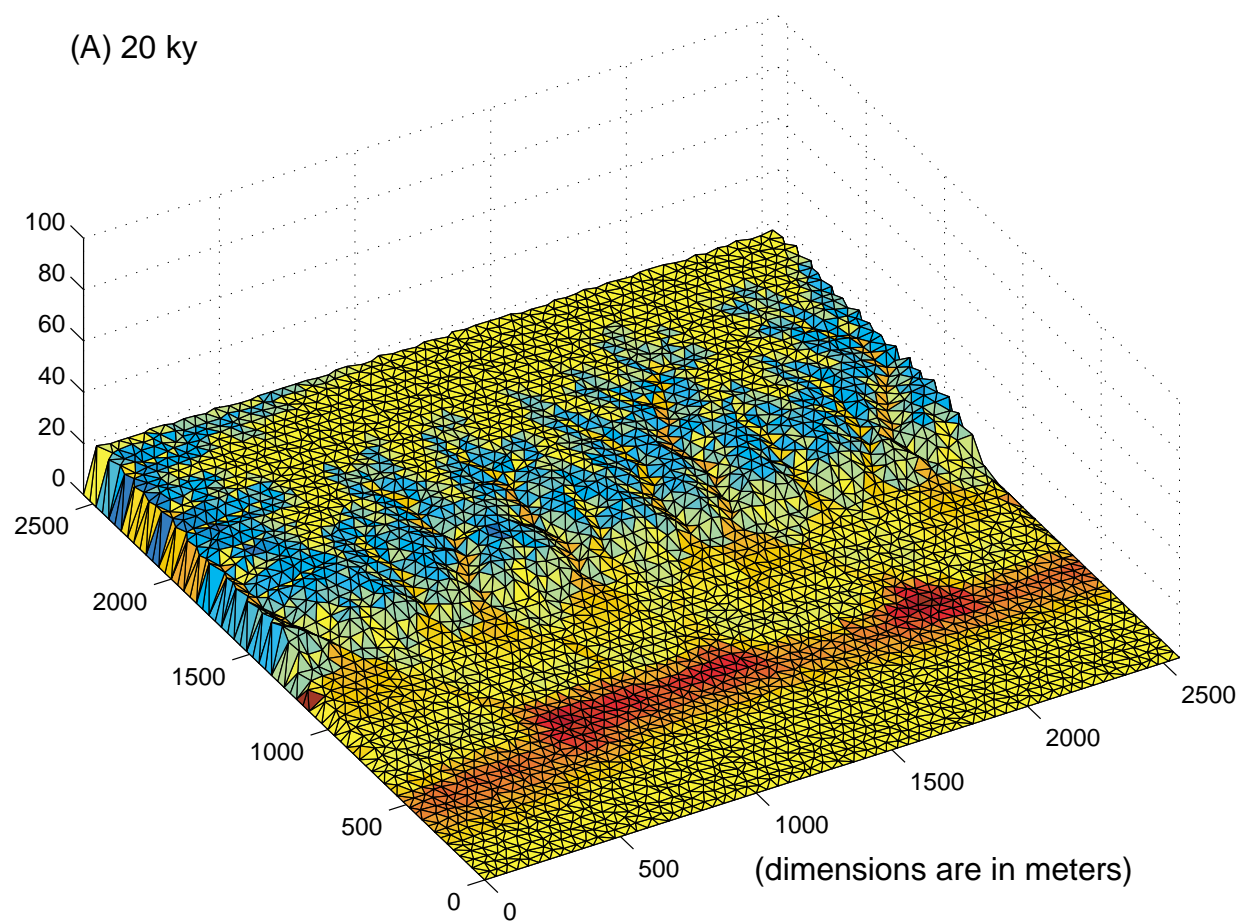


Figure 9b

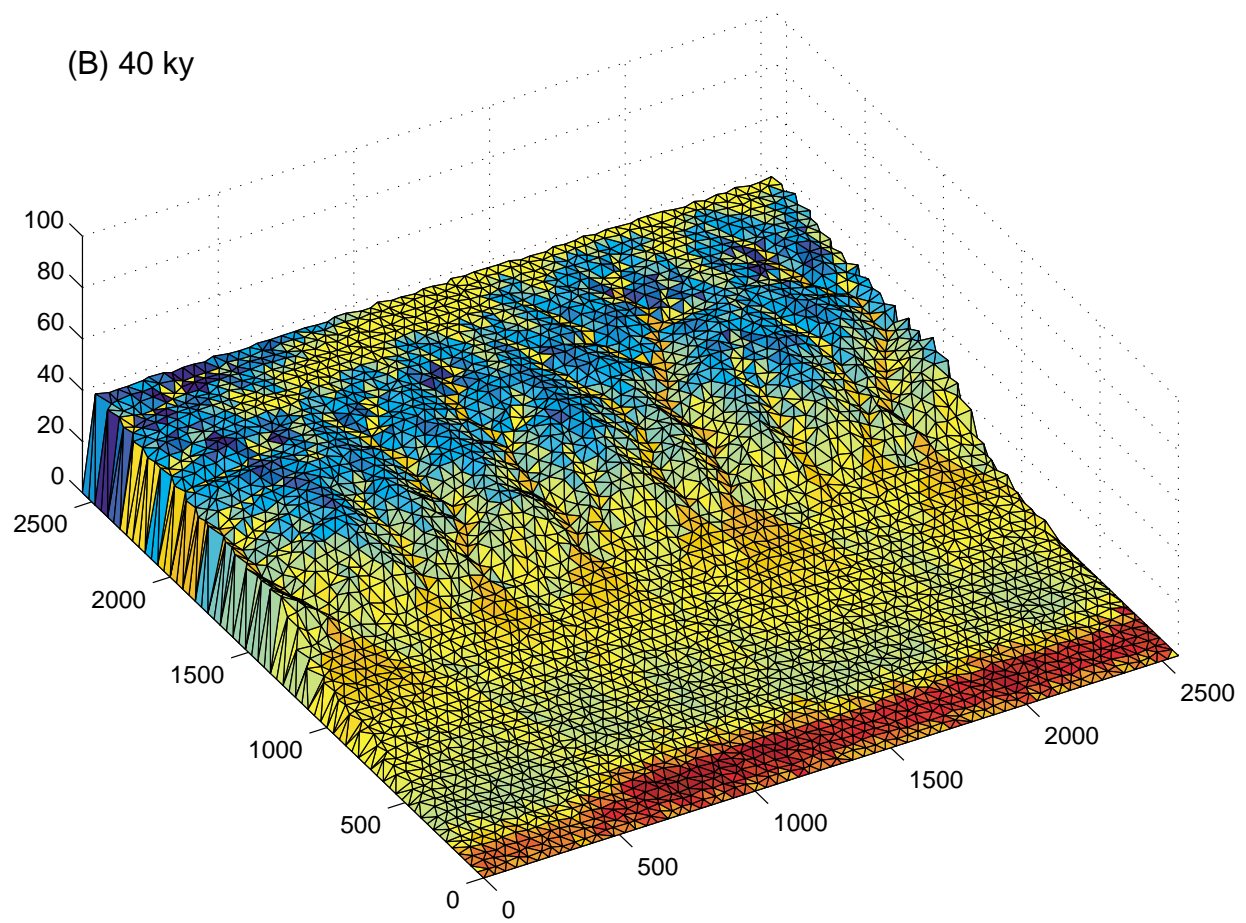


Figure 9c

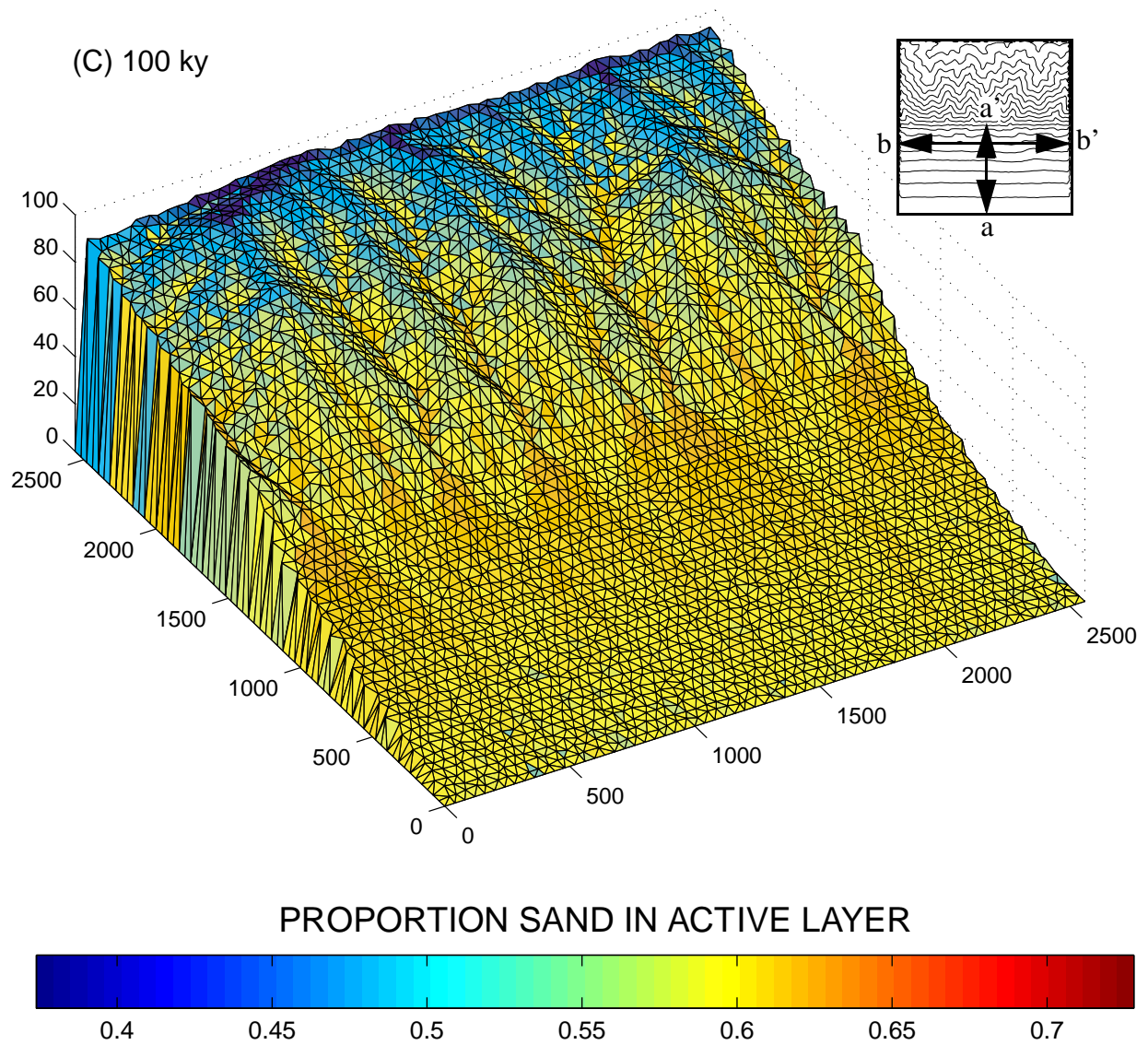


Figure 10

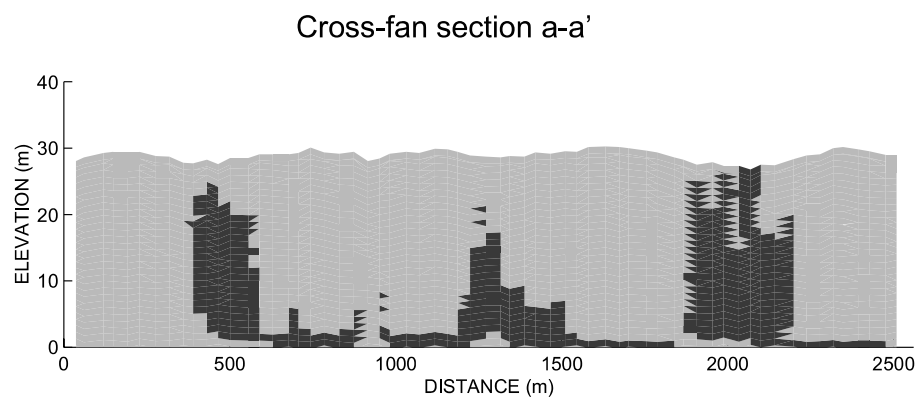


Figure 11

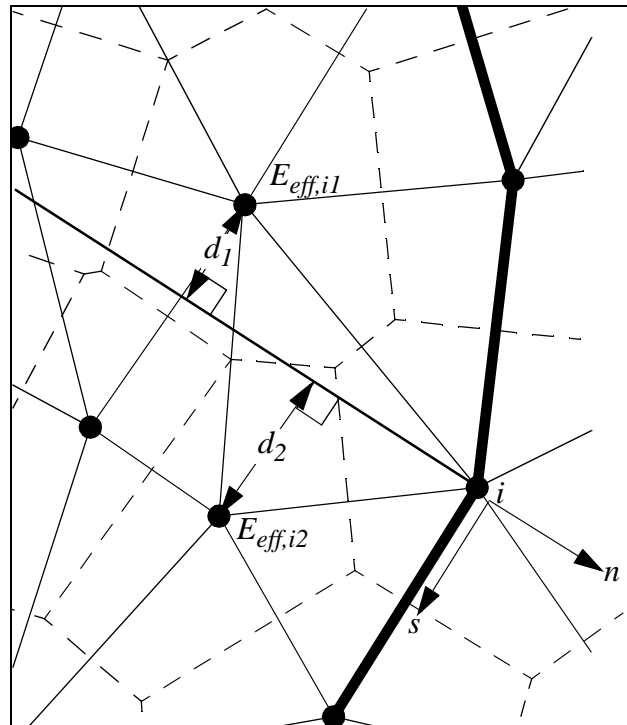


Figure 12

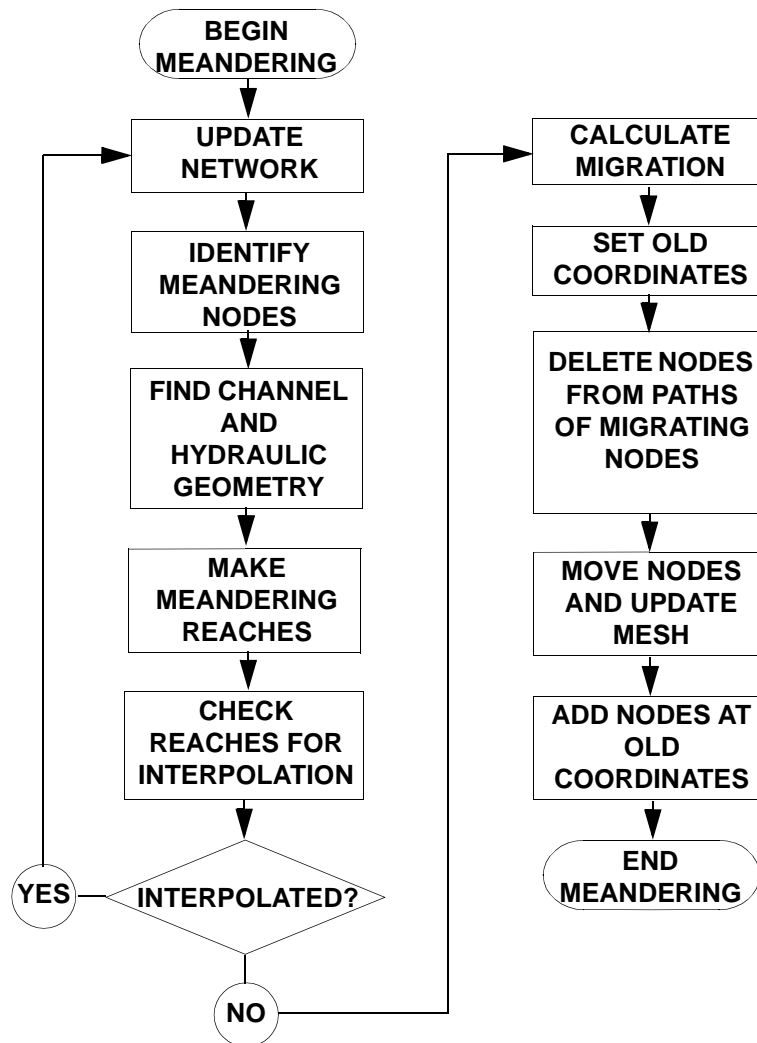




Figure 13

